

A LOW-DEGREE STRICTLY CONSERVATIVE FINITE ELEMENT METHOD FOR INCOMPRESSIBLE FLOWS

HUILAN ZENG, CHEN-SONG ZHANG, AND SHUO ZHANG

ABSTRACT. In this paper, a new $P_2 - P_1$ finite element pair is proposed for incompressible fluid. For this pair, the discrete inf-sup condition and the discrete Korn's inequality hold on general triangulations. It yields exactly divergence-free velocity approximations when applied to models of incompressible flows. The robust capacity of the pair for incompressible flows are verified theoretically and numerically.

1. INTRODUCTION

The property of conservation plays a key role in the modeling of many physical systems. For the Stokes problem, for example, if a stable finite element pair can inherit the mass conservation, the approximation of the velocity can be independent of the pressure and the method does not suffer from the locking effect with respect to large Reynolds' numbers (c.f., e.g., [8]). The importance of conservative schemes is also significant in, e.g., the nonlinear mechanics [2, 3] and the magnetohydrodynamics [24, 26, 27]. In this paper, we focus on the conservative scheme for the Stokes-type problems for incompressible flows. As Stokes-type problems are applied widely to not only fluid problems but also elastic models such as the earth model with a fluid core [13] and they are immediately related to many other model problems, their conservative schemes can be relevant and helpful to more other equations.

Most classical stable Stokes pairs relax the divergence-free constraint by enforcing the condition in the weak sense, and the conservation can be preserved strictly only for special examples. Though, during the past decade, the conservative schemes have been recognized more clearly as *pressure robustness* and widely studied and surveyed in, e.g., [18, 22, 29, 36]. This conservation is also related to other key features such as “viscosity-independent” [40] and “gradient-robustness” [31] for numerical schemes. There have been various successful examples along different technical approaches. Efforts have been devoted to the construction of conforming conservative pairs, and extra structural assumptions are generally needed for the subdivision and finite element functions. Examples include conforming elements designed for special meshes, such as $P_k - P_{k-1}$ triangular elements for $k \geq 4$ on singular-vertex-free meshes [37] and for smaller k constructed on composite grids [1, 35, 37, 43, 46], and the pairs given in [16, 22] which work for general triangulations but with extra smoothness requirement and more complicated shape

2000 *Mathematics Subject Classification.* Primary 65N12, 65N30, 76D05.

Key words and phrases. Incompressible (Navier-)Stokes equations; Brinkman equations; inf-sup condition; discrete Korn's inequality, strictly conservative scheme; pressure-robust discretization.

This work is supported by the Strategic Priority Research Program of Chinese Academy of Sciences (XDB 41000000), National Key R&D Program of China (2020YFA0711904), and the Natural Science Foundation of China (11871465 and 11971472).

function spaces. A natural way to relax the constraints is to use $H(\text{div})$ -conforming but $(H^1)^2$ -nonconforming finite element functions for the velocity. For example, in [33], a reduced cubic polynomial space which is $H(\text{div})$ -conforming and $(H^1)^2$ -nonconforming is used for the velocity and piecewise constant for the pressure. The pair is both stable and conservative on general triangulations. The velocity space of [33] can be recognized as a modification of an $H(\text{div})$ -conforming space by adding some normal-bubble-like functions to enforce weak continuity of tangential component. Several conservative pairs are constructed subsequently in, e.g., [20, 39, 41]. Generally, to construct a conservative pair that works on general triangulations without special structures, cubic and higher-degree polynomials are used for the velocity. Besides, For conservative pairs in three-dimension, we refer to, e.g., [23, 45, 49] where composite grids are required, as well as [21, 48] where high degree local polynomials are utilized. We refer to [10, 28, 47] for rectangular grids and [34] for cubic grids where full advantage of the geometric symmetry of the cells are taken.

In this paper, we propose a new $P_2 - P_1$ finite element pair on triangulations; for the velocity field, we use piecewise quadratic $H(\text{div})$ functions whose tangential component is continuous in the average sense, and for the pressure, we use discontinuous piecewise linear functions. The pair is stable and immediately strictly conservative on general triangulations. Further, a discrete Korn's inequality holds for the velocity. The capability of the pair is verified both theoretically and numerically. When applied to the Stokes and the Darcy–Stokes–Brinkman problems, the approximation of the velocity is independent of the small parameters and thus locking-free; numerical experiments verify the validity of the theory. We note that, as the tangential component of the velocity function is continuous only in the average sense, the convergence rate can only be proved to be of $O(h)$ order. However, since the pair is conservatively stable on general triangulations, it plays superior to some $O(h^2)$ schemes numerically in robustness with respect to triangulations and with respect to small parameters. The performance of the pair on the Navier–Stokes equation is also illustrated numerically. More applications in other model problems for both the source problems and the eigenvalue problems may be studied in future.

For the newly designed space for velocity, all the degrees of freedom are located on edges of the triangulation. It is thus impossible to construct a commutative nodal interpolator with a non-constant pressure space. To prove the inf-sup condition, we adopt Stenberg's macroelement technique [38]. On every macroelement, the surjection property of the divergence operator is confirmed by figuring out its kernel space. This figures out a structure of discretized Stokes complex on any local macroelements. On the other hand, similar to the study of conservative pairs in [16, 22] and the study of biharmonic finite elements in [15, 44, 50, 51], the proposed global space will be embedded in a discretized Stokes complex on the whole triangulation; this will be studied in detail in future.

The method given uses an $H(\text{div})$ -conforming and $(H^1)^2$ -nonconforming finite element for the velocity. Indeed, the space given here is a reduced subspace of the second order Brezzi–Douglas–Marini element [7] space by enhancing smoothness. This way, the proposed pair is different from most existing $H(\text{div})$ -conforming and $(H^1)^2$ -nonconforming methods which propose to add bubble-like basis functions on some specific $H(\text{div})$ finite element space. Moreover, as we use quadratic polynomials only for velocity, to the best of our knowledge, this is the lowest-degree

conservative stable pair for the Stokes problem on general triangulations. More stable and conservative pairs may be designed by reducing other $H(\text{div})$ -conforming elements. The possible generalization of the proposed pair to three-dimensional case will also be discussed.

Finally we remark that, besides these finite element methods mentioned above, an alternative is to construct specially discrete variational forms onto $H(\text{div})$ functions where extra stabilizations may play roles; works such as the discontinuous Galerkin method, the weak Galerkin method, and the virtual element method all fall into this category. There have been many valuable works of these types, but we do not seek to give a complete survey and thus will not discuss them in the present paper. We only note that natural connections between the proposed pair and DG-type methods may be expected under the framework of [25]; along the lines of [14], these connections may be expected helpful for the construction of optimal solvers for the DG schemes.

The rest of the paper is organized as follows. At the remaining of this section, some notations are given. In Section 2, a new $P_2 - P_1$ element method is proposed, and significant properties of it are presented. In Sections 3, the convergence analysis of the element applied to the Stokes problem and the Darcy-Stokes-Brinkman problem is provided. In Section 4, numerical experiments are presented to reflect the efficiency of the strictly conservative method when compared with some classical elements. A meticulous proof of a significant lemma devoted to the verification of the inf-sup condition is put in Appendix A.

1.1. Notations. Throughout this paper, Ω is a bounded and connected polygonal domain in \mathbb{R}^2 . We use ∇ , Δ , div , rot , curl to denote the gradient, Laplace, divergence, rotation, and curl operators, respectively. As usual, we use $L^p(\Omega)$, $H^s(\Omega)$, $H(\text{div}, \Omega)$, $H(\text{rot}, \Omega)$, $H_0^s(\Omega)$, and $H_0(\text{div}, \Omega)$ for standard Sobolev spaces. Denote $L_0^2(\Omega) := \{w \in L^2(\Omega) : \int_{\Omega} w d\Omega = 0\}$. We use “ $\underline{\quad}$ ” for vector valued quantities. Specifically, we denote $\underline{L}^p(\Omega) := (L^p(\Omega))^2$, $\underline{H}^s(\Omega) := (H^s(\Omega))^2$, $\underline{H}(\text{div}, \Omega) := (H(\text{div}, \Omega))^2$, and $\underline{H}(\text{rot}, \Omega) := (H(\text{rot}, \Omega))^2$. Denote, by $H^{-s}(\Omega)$ and $\underline{H}^{-s}(\Omega)$, the dual spaces of $H_0^s(\Omega)$ and $\underline{H}_0^s(\Omega)$, respectively. We utilize the subscript “ \cdot_h ” to indicate the dependence on grids. Particularly, an operator with the subscript “ \cdot_h ” implies the operation is done cell by cell. We denote (\cdot, \cdot) and $\langle \cdot, \cdot \rangle$ as the usual inner product and the dual product, respectively. Finally, \lesssim , \gtrsim , and \approx respectively denote \leq , \geq , and $=$ up to some multiplicative generic constant [42], which only depends on the domain and the shape-regularity of subdivisions.

Let $\{\mathcal{T}_h\}$ be in a family of triangular grids of domain Ω . The boundary $\partial\Omega = \Gamma_D \cup \Gamma_N$. Let \mathcal{N}_h be the set of all vertices, $\mathcal{N}_h = \mathcal{N}_h^i \cup \mathcal{N}_h^b$, with \mathcal{N}_h^i and \mathcal{N}_h^b comprising the interior vertices and the boundary vertices, respectively. Similarly, let $\mathcal{E}_h = \mathcal{E}_h^i \cup \mathcal{E}_h^b$ be the set of all the edges, with \mathcal{E}_h^i and \mathcal{E}_h^b comprising the interior edges and the boundary edges, respectively. For an edge e , \mathbf{n}_e is a unit vector normal to e and \mathbf{t}_e is a unit tangential vector of e such that $\mathbf{n}_e \times \mathbf{t}_e > 0$. On the edge e , we use $[[\cdot]]_e$ for the jump across e . We stipulate that, if $e = T_1 \cap T_2$, then $[[v]]_e = (v|_{T_1} - v|_{T_2})|_e$ if the direction of \mathbf{n}_e goes from T_1 to T_2 , and if $e \subset \partial\Omega$, then $[[\cdot]]_e$ is the evaluation on e .

Suppose that T represents a triangle in \mathcal{T}_h . Let h_T and ρ_T be the circumscribed radius and the inscribed circles radius of T , respectively. Let $h := \max_{T \in \mathcal{T}_h} h_T$ be the mesh size of \mathcal{T}_h . Let $P_l(T)$ denote the space of polynomials on T of the total degree no more than l . Similarly, we define the

space $P_l(e)$ on an edge e . We assume that $\{\mathcal{T}_h\}$ is a family of regular subdivisions, i.e.,

$$(1.1) \quad \max_{T \in \mathcal{T}_h} \frac{h_T}{\rho_T} \leq \gamma_0,$$

where γ_0 is a generic constant independent of h .

2. A NEW $P_2 - P_1$ FINITE ELEMENT PAIR

2.1. Construction of a new finite element pair. Let T be a triangle with nodes $\{a_i, a_j, a_k\}$, and e_i be an edge of T opposite to the i -th vertex a_i ; see Figure 1. Denote a unit vector normal to e_i and a unit tangential vector of e_i as \mathbf{n}_{T,e_i} and \mathbf{t}_{T,e_i} , respectively.

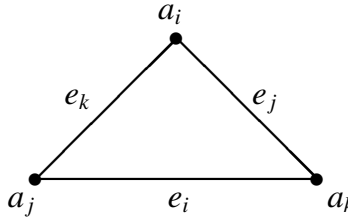


FIGURE 1. Illustration of a triangle and its nodes and edges.

The new vector P_2 element is defined by the triple (T, P_T, D_T) :

- (1) T is a triangle;
- (2) $P_T := (P_2(T))^2$;
- (3) for any $\underline{v} \in (H^1(T))^2$, the degrees of freedom on T , denoted by D_T , are

$$\left\{ \int_{e_i} \underline{v} \cdot \mathbf{n}_{T,e_i} ds, \int_{e_i} \underline{v} \cdot \mathbf{n}_{T,e_i} (\lambda_j - \lambda_k) ds, \int_{e_i} \underline{v} \cdot \mathbf{n}_{T,e_i} (-\lambda_j \lambda_k + \frac{1}{6}) ds, \int_{e_i} \underline{v} \cdot \mathbf{t}_{T,e_i} ds \right\}_{i=1:3},$$

where $\{\lambda_i, \lambda_j, \lambda_k\}$ represent the barycentric coordinates on T . The above triple is P_T -unisolvent. Particularly, we use $\underline{\varphi}_{\mathbf{n}_{T,e_i},0}$, $\underline{\varphi}_{\mathbf{n}_{T,e_i},1}$, $\underline{\varphi}_{\mathbf{n}_{T,e_i},2}$, and $\underline{\varphi}_{\mathbf{t}_{T,e_i},0}$ to represent the nodal basis functions associated with DOFs on e_i , and then

$$(2.1) \quad \begin{cases} \underline{\varphi}_{\mathbf{n}_{T,e_i},0} = \lambda_j(3\lambda_j - 2) \frac{\mathbf{t}_k}{(\mathbf{n}_i, \mathbf{t}_k)} + \lambda_k(3\lambda_k - 2) \frac{\mathbf{t}_j}{(\mathbf{n}_i, \mathbf{t}_j)} + 6\lambda_j \lambda_k \mathbf{n}_i; \\ \underline{\varphi}_{\mathbf{n}_{T,e_i},1} = 3\lambda_j(3\lambda_j - 2) \frac{\mathbf{t}_k}{(\mathbf{n}_i, \mathbf{t}_k)} - 3\lambda_k(3\lambda_k - 2) \frac{\mathbf{t}_j}{(\mathbf{n}_i, \mathbf{t}_j)}; \\ \underline{\varphi}_{\mathbf{n}_{T,e_i},2} = 30\lambda_j(3\lambda_j - 2) \frac{\mathbf{t}_k}{(\mathbf{n}_i, \mathbf{t}_k)} + 30\lambda_k(3\lambda_k - 2) \frac{\mathbf{t}_j}{(\mathbf{n}_i, \mathbf{t}_j)}; \\ \underline{\varphi}_{\mathbf{t}_{T,e_i},0} = 6\lambda_j \lambda_k \mathbf{t}_i. \end{cases}$$

The corresponding finite element space is defined by

$$\underline{V}_h := \left\{ \underline{v}_h \in \underline{L}^2(\Omega) : \underline{v}_h|_T \in (P_2(T))^2, \forall T \in \mathcal{T}_h; \underline{v}_h \cdot \mathbf{n}_e \text{ and } \int_e \underline{v}_h \cdot \mathbf{t}_e ds \text{ are continuous } \forall e \in \mathcal{E}_h^i \right\}.$$

Note that $\underline{V}_h \subset \underline{H}(\text{div}, \Omega)$ but $\underline{V}_h \not\subset \underline{H}^1(\Omega)$.

Define a nodal interpolation operator $\Pi_h : \underline{H}^1(\Omega) \rightarrow \underline{V}_h$ such that for any $e \in \mathcal{E}_h$,

$$\begin{aligned} \int_e \Pi_h \underline{v} \cdot \mathbf{n}_e w ds &= \int_e \underline{v} \cdot \mathbf{n}_e w ds, \quad \forall w \in P_2(e), \\ \int_e \Pi_h \underline{v} \cdot \mathbf{t}_e ds &= \int_e \underline{v} \cdot \mathbf{t}_e ds. \end{aligned}$$

The operator Π_h is locally defined, and the local space $\underline{V}_h(T)$ restricted on T is invariant under the Piola's transformation, i.e., it maps $\underline{V}_h(T)$ onto $\underline{V}_h(\hat{T})$, where \hat{T} represents a reference triangle. Moreover, Π_h preserves quadratic functions locally. Therefore, a combination of Lemmas 1.6 and 1.7 in [8], standard scaling arguments, and the Bramble-Hilbert lemma leads to the following approximation property of Π_h .

Proposition 2.1. *If $0 \leq k \leq 1 \leq s \leq 3$, then*

$$(2.2) \quad \|\underline{v} - \Pi_h \underline{v}\|_{k,h} \lesssim h^{s-k} \|\underline{v}\|_{s,\Omega}, \quad \forall \underline{v} \in \underline{H}^s(\Omega).$$

Moreover, the following low order estimate is valid

$$(2.3) \quad \|\underline{v} - \Pi_h \underline{v}\|_{0,\Omega} \lesssim h^{1/2} \|\underline{v}\|_{0,\Omega} \|\underline{v}\|_{1,\Omega}.$$

Assume Γ_D to be a part of the boundary $\partial\Omega$. Define

$$\begin{aligned} \underline{V}_{hD} := \{ \underline{v}_h \in \underline{L}^2(\Omega) : \underline{v}_h|_T \in (P_2(T))^2, \forall T \in \mathcal{T}_h; \underline{v}_h \cdot \mathbf{n}_e \text{ and } \int_e \underline{v}_h \cdot \mathbf{t}_e ds \\ \text{are continuous for any } e \in \mathcal{E}_h^i \text{ and vanish for any } e \subset \Gamma_D \}. \end{aligned}$$

Specially, if $\Gamma_D = \partial\Omega$, \underline{V}_{hD} is written as \underline{V}_{h0} . Define

$$Q_h := \{q \in L^2(\Omega) : q|_T \in P_1(T), \forall T \in \mathcal{T}_h\}, \quad \text{and } Q_{h*} := Q_h \cap L_0^2(\Omega).$$

Evidently, $\text{div } \underline{V}_h \subset Q_h$. Therefore, $\underline{V}_{hD} \times Q_h$ and $\underline{V}_{h0} \times Q_{h*}$ each forms a conservative pair. The stability and discrete Korn's inequality also hold. We firstly introduce an assumption on the triangulations.

Assumption A. Every triangle in \mathcal{T}_h has at least one vertex in the interior of Ω .

The theorems below, which will be proved in the sequel subsections, hold on triangulations that satisfy **Assumption A**.

Theorem 2.2 (Inf-sup conditions). *Let $\{\mathcal{T}_h\}$ be a family of triangulations satisfying **Assumption A**. Then*

$$(2.4) \quad \sup_{\underline{v}_h \in \underline{V}_{hD}} \frac{\int_{\Omega} \text{div } \underline{v}_h q_h d\Omega}{\|\underline{v}_h\|_{1,h}} \gtrsim \|q\|_{0,\Omega}, \quad \forall q \in Q_h, \quad \text{if } \Gamma_D \neq \partial\Omega,$$

$$(2.5) \quad \sup_{\underline{v}_h \in \underline{V}_{h0}} \frac{\int_{\Omega} \text{div } \underline{v}_h q_h d\Omega}{\|\underline{v}_h\|_{1,h}} \gtrsim \|q\|_{0,\Omega}, \quad \forall q \in Q_{h*}.$$

Theorem 2.3 (Discrete Korn's inequality). *Let $\{\mathcal{T}_h\}$ be a family of triangulations satisfying **Assumption A**. Let $\epsilon(\underline{v}) := \frac{1}{2}[\nabla \underline{v} + (\nabla \underline{v})^T]$. Then*

$$(2.6) \quad \sum_{T \in \mathcal{T}_h} \int_T |\epsilon(\underline{v})|^2 dT \gtrsim \|\underline{v}\|_{1,h}^2, \quad \forall \underline{v} \in \underline{V}_{hD}.$$

2.2. Proof of inf-sup conditions. Note that the commutativity $\operatorname{div} \Pi_h \underline{w} = P_{Q_{h^*}} \operatorname{div} \underline{w}$ does not hold for all $\underline{w} \in \underline{H}_0^1(\Omega)$, where $P_{Q_{h^*}}$ represents the L^2 projection onto Q_{h^*} . To prove the inf-sup conditions (2.4) and (2.5), we adopt the macroelement technique by Stenberg [38]. We postpone the proof of Theorem 2.2 after some technical preparations.

2.2.1. Stenberg's macroelement technique. A macroelement is a connected set of at least two cells in \mathcal{T}_h . And a macroelement partition of \mathcal{T}_h , denoted by \mathcal{M}_h , is a set of macroelements such that each triangle in of \mathcal{T}_h is covered by at least one macroelement in \mathcal{M}_h .

Definition 2.4. Two macroelements M_1 and M_2 are said to be equivalent if there exists a continuous one-to-one mapping $G : M_1 \rightarrow M_2$, such that

- (a) $G(M_1) = M_2$;
- (b) if $M_1 = \cup_{i=1}^m T_i^1$, then $T_i^2 = G(T_i^1)$ with $i = 1 : m$ are the cells of M_2 .
- (c) $G|_{T_i^1} = F_{T_i^2} \circ F_{T_i^1}^{-1}$, $i = 1 : m$, where $F_{T_i^1}$ and $F_{T_i^2}$ are the mappings from a reference element \hat{T} onto T_i^1 and T_i^2 , respectively.

A class of equivalent macroelements is a set of all the macroelements which are equivalent to each other. Given a macroelement M , we denote

$$\underline{V}_{h0,M} := \underline{V}_{h0}(M), \quad Q_{h,M} := Q_h(M), \quad \text{and} \quad Q_{h^*,M} := Q_{h^*}(M).$$

And we denote

$$(2.7) \quad N_M := \left\{ q_h \in Q_{h,M} : \int_M \operatorname{div} \underline{v}_h q_h dM = 0, \forall \underline{v}_h \in \underline{V}_{h0,M} \right\}.$$

Stenberg's macroelement technique can be summarized as the following proposition.

Proposition 2.5. [38, Theorem 3.1] *Suppose there exist a macroelement partitioning \mathcal{M}_h with a fixed set of equivalence classes \mathbb{E}_i of macroelements, $i = 1, 2, \dots, n$, a positive integer N (n and N are independent of h), and an operator $\Pi : \underline{H}_0^1(\Omega) \rightarrow \underline{V}_{h0}$, such that*

- (C₁) *for each $M \in \mathbb{E}_i$, $i = 1, 2, \dots, n$, the space N_M defined in (2.7) is one-dimensional, which consists of functions that are constant on M ;*
- (C₂) *each $M \in \mathcal{M}_h$ belongs to one of the classes \mathbb{E}_i , $i = 1, 2, \dots, n$;*
- (C₃) *each $e \in \mathcal{E}_h^i$ is an interior edge of at least one and no more than N macroelements;*
- (C₄) *for any $\underline{w} \in \underline{H}_0^1(\Omega)$, it holds that*

$$\sum_{T \in \mathcal{T}_h} h_T^{-2} \|\underline{w} - \Pi \underline{w}\|_{0,T}^2 + \sum_{e \in \mathcal{E}_h^i} h_e^{-1} \|\underline{w} - \Pi \underline{w}\|_{0,e}^2 \lesssim \|\underline{w}\|_{1,\Omega}^2 \quad \text{and} \quad \|\Pi \underline{w}\|_{1,h} \lesssim \|\underline{w}\|_{1,\Omega}.$$

Then the stability (2.5) is valid.

2.2.2. Technical lemmas. In general, the main difficulty to design a stable mixed element stems from (C₁). We use the specific type of macroelements as below.

Definition 2.6. A macroelement, denoted by M , being a union of the m cells that share exactly one common vertex in the interior of the macroelement, is called an **m-cell vertex-centred macroelement**, and **m-macroelement** for short.

The set of interior edges and cells of M are denoted by $\{e_i\}_{i=1:m}$ and $\{T_i\}_{i=1:m}$, respectively. Denote the lengths of interior edges by $\{d_i\}_{i=1:m}$ and the areas of cells by $\{S_i\}_{i=1:m}$. Figure 2 gives an illustration of a **6-macroelement**.

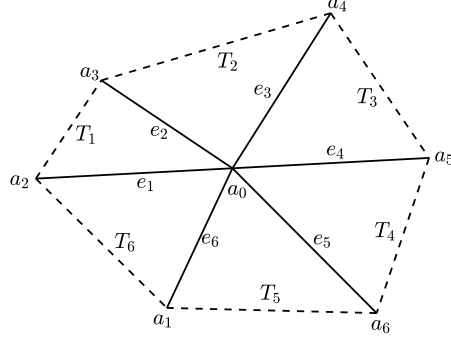


FIGURE 2. A macroelement composed of six cells with one interior vertex

Below are concrete definitions of some local defined spaces on M introduced in the previous context.

$$\underline{V}_{h0,M} := \left\{ \underline{v}_h \in \underline{L}^2(M) : \underline{v}_h|_T \in (P_2(T))^2, \forall T \subset M, \underline{v}_h \cdot \mathbf{n}_e \text{ and } \int_e \underline{v}_h \cdot \mathbf{t}_e ds \text{ are continuous across interior edges and vanish on } \partial M \right\},$$

$$\underline{Q}_{h,M} = \{ q_h \in L^2(M) : q_h|_T \in P_1(T), \forall T \in M \},$$

$$\underline{Q}_{h^*,M} = \{ q_h \in \underline{Q}_{h,M} : \int_M q_h dM = 0 \}.$$

For an **m-macroelement** M , denote by $\ker(\operatorname{div}, \underline{V}_{h0,M}) := \{ \underline{v}_h \in \underline{V}_{h0,M} : \operatorname{div} \underline{v}_h = 0 \}$ and $\operatorname{Im}(\operatorname{div}, \underline{V}_{h0,M}) = \operatorname{div}(\underline{V}_{h0,M})$. The main technical issue is the following lemma.

Lemma 2.7. *It holds that $\dim(\ker(\operatorname{div}, \underline{V}_{h0,M})) \leq m + 1$.*

We postpone the technical proof of Lemma 2.7 to Appendix A.

Lemma 2.8. *Let M be an m-macroelement. Then N_M is a one-dimensional space consisting of constant functions on M .*

Proof. First we show $\operatorname{Im}(\operatorname{div}, \underline{V}_{h0,M}) = \underline{Q}_{h^*,M}$. As $\dim \underline{V}_{h0,M} = \dim(\ker(\operatorname{div}, \underline{V}_{h0,M})) + \dim(\operatorname{Im}(\operatorname{div}, \underline{V}_{h0,M}))$, we obtain $\dim(\operatorname{Im}(\operatorname{div}, \underline{V}_{h0,M})) \geq 3m - 1$, where we have utilized $\dim \underline{V}_{h0,M} = 4m$ by definition and $\dim(\ker(\operatorname{div}, \underline{V}_{h0,M})) \leq m + 1$ by Lemma 2.7. From $\dim(\underline{Q}_{h^*,M}) = 3m - 1$ and $\operatorname{Im}(\operatorname{div}, \underline{V}_{h0,M}) \subset \underline{Q}_{h^*,M}$, we derive $\operatorname{Im}(\operatorname{div}, \underline{V}_{h0,M}) = \underline{Q}_{h^*,M}$. Then, for any $q_h \in N_M$, it holds that $\int_M p_h^* q_h dM = 0$, for any $p_h^* \in \underline{Q}_{h^*,M}$. Let $q_h = \bar{q}_h + q_h^*$, where $\bar{q}_h = \int_M q_h dM$ and $q_h^* \in \underline{Q}_{h^*,M}$. Then $\int_M p_h^* q_h^* dM = 0$, $\forall p_h^* \in \underline{Q}_{h^*,M}$, which yields $q_h^* = 0$ and hence $q_h = \bar{q}_h$. Therefore, N_M is a one-dimensional space consisting of constant functions on M . \square

Lemma 2.9. *Let $\{\mathcal{T}_h\}$ be a family of triangulations satisfying **Assumption A**. Each macroelement in \mathcal{M}_h has one interior vertex. Then conditions C_2 , C_3 , and C_4 in Theorem 2.5 are satisfied.*

Proof. From the **Assumption A** and the regularity (1.1) of \mathcal{T}_h , there exists a generic constant n , independent of h , such that condition C_2 holds. If $e \in \mathcal{E}_h^i$, then at least one endpoint of e is an interior vertex. Hence e is an interior edge of at least one macroelement of \mathcal{M}_h . On the other hand, e is interior to at most two macroelements, which occurs if both endpoints of e are interior in Ω .

Therefore, condition C_3 also holds. By Proposition 2.1 and the well-known trace theorem (see, e.g., [5, Theorem 1.6.6]), condition C_4 can be obtained. \square

2.2.3. Proof of Theorem 2.2. By Lemma 2.8, Lemma 2.9, and Theorem 2.5, it holds that $\underline{V}_{h0} \times \underline{Q}_{h*}$ satisfies the inf-sup condition (2.5). The inf-sup stability of $\underline{V}_{hD} \times \underline{Q}_h$ is proved utilizing the technique introduced in [30] by the following four steps.

Step 1. Given $q_h \in \underline{Q}_h$, let $\bar{q}_h = \frac{1}{|\Omega|} \int_{\Omega} q_h d\Omega$ and $q_h^* = q_h - \bar{q}_h$. Then $q_h^* \in L_0^2(\Omega)$ and

$$(2.8) \quad \|q_h\|_{0,\Omega}^2 = \|\bar{q}_h\|_{0,\Omega}^2 + \|q_h^*\|_{0,\Omega}^2.$$

Step 2. By (2.5), there exists some $\underline{v}_h^* \in \underline{V}_{h0}$, such that

$$(2.9) \quad (\operatorname{div} \underline{v}_h^*, q_h^*) \geq C_1 \|q_h^*\|_{0,\Omega}^2 \quad \text{and} \quad |\underline{v}_h^*|_{1,h} = \|q_h^*\|_{0,\Omega},$$

where $C_1 > 0$ is a generic constant independent of h .

Step 3. Let $\Gamma_N := \partial\Omega \setminus \Gamma_D$. Notice that \bar{q}_h is constant in Ω . Let $\bar{v}_h \in \underline{V}_{hD}$ satisfy that $\bar{v}_h \cdot \mathbf{n}_e = C_0 \bar{q}_h|_e$ for any $e \subset \Gamma_N$, and other degrees of freedom vanish. The value of C_0 is chosen such that $|\bar{v}_h|_{1,h} = \|\bar{q}_h\|_{0,\Omega}$. Then it holds with $C_2 := C_0 \frac{|\Gamma_N|}{|\Omega|}$ that

$$(2.10) \quad (\operatorname{div} \bar{v}_h, \bar{q}_h) = \sum_{T \in \mathcal{T}_h} \int_T \operatorname{div} \bar{v}_h \bar{q}_h dT = \sum_{e \in \Gamma_N} \int_e \bar{v}_h \cdot \mathbf{n} \bar{q}_h ds = C_2 \|\bar{q}_h\|_{0,\Omega}^2.$$

Step 4. Let $\underline{v}_h = \underline{v}_h^* + \kappa \bar{v}_h$ with $\kappa = \frac{2C_1 C_2}{(C_2)^2 + 2}$. By the Schwarz inequality, the elementary inequality, and (2.8)–(2.10), we obtain

$$\begin{aligned} (\operatorname{div} \underline{v}_h, q_h) &= (\operatorname{div} \underline{v}_h^*, q_h^*) + \kappa (\operatorname{div} \bar{v}_h, \bar{q}_h) + \kappa (\operatorname{div} \bar{v}_h, q_h^*) \\ &\geq C_1 \|q_h^*\|_{0,\Omega}^2 + C_2 \kappa \|\bar{q}_h\|_{0,\Omega}^2 + \kappa (\operatorname{div} \bar{v}_h, q_h^*) \\ &\geq C_1 \|q_h^*\|_{0,\Omega}^2 + C_2 \kappa \|\bar{q}_h\|_{0,\Omega}^2 - \sqrt{2} \kappa \left(\frac{C_2}{2\sqrt{2}} |\bar{v}_h|_{1,h}^2 + \frac{\sqrt{2}}{2C_2} \|q_h^*\|_{0,\Omega}^2 \right) \\ &= \left(C_1 - \frac{\kappa}{C_2} \right) \|q_h^*\|_{0,\Omega}^2 + \frac{C_2 \kappa}{2} \|\bar{q}_h\|_{0,\Omega}^2 = \frac{C_1 (C_2)^2}{(C_2)^2 + 2} \|q_h\|_{0,\Omega}^2. \end{aligned}$$

From $|\underline{v}_h^*|_{1,h} = \|q_h^*\|_{0,\Omega}$, $|\bar{v}_h|_{1,h} = \|\bar{q}_h\|_{0,\Omega}$, and the Poincaré inequality, we have $\|\underline{v}_h\|_{1,h} \lesssim \|q_h\|_{0,\Omega}$. This completes the proof of (2.4) and Theorem 2.2.

2.3. Proof of discrete Korn's inequality. To verify the discrete Korn's inequality, we follow the lines of [30] and firstly introduce an auxiliary element scheme constructed by adding element bubble functions to the the standard Bernardi-Raugel element [4]. Denote

$$\underline{P}_T := (P_1(T))^2 \oplus \operatorname{span}\{\lambda_2 \lambda_3 \mathbf{n}_1, \lambda_3 \lambda_1 \mathbf{n}_2, \lambda_1 \lambda_2 \mathbf{n}_3\} \oplus (\operatorname{span}\{\lambda_1 \lambda_2 \lambda_3\})^2.$$

Define

$$\begin{aligned} \underline{C}_h &:= \{ \underline{z}_h \in \underline{H}^1(\Omega) : \underline{z}_h|_T \in \underline{P}_T, \forall T \in \mathcal{T}_h, \underline{z}_h(a) \text{ is continuous at any } a \in \mathcal{N}_h^i, \\ &\quad \text{and } \int_e \underline{z}_h \cdot \mathbf{n}_e ds \text{ is continuous across any } e \in \mathcal{E}_h^i \}, \end{aligned}$$

and $\underline{C}_h^N := \{ \underline{z}_h \in \underline{C}_h : \underline{z}_h(a) = 0, \forall a \in \Gamma_N \text{ and } \int_e \underline{z}_h \cdot \mathbf{n}_e ds = 0, \forall e \subset \Gamma_N \}$, where $\Gamma_N = \partial\Omega \setminus \Gamma_D$. Here we are concerned about the case of $\Gamma_D \neq \partial\Omega$, in which the discrete Korn's inequality plays a crucial role for outflow conditions.

2.3.1. Technical lemmas.

Lemma 2.10. *The element pair $\underline{C}_h^N \times Q_h$ satisfies the inf-sup condition*

$$(2.11) \quad \sup_{\underline{z}_h \in \underline{C}_h^N} \frac{\int_{\Omega} \operatorname{div} \underline{z}_h q_h d\Omega}{|\underline{z}_h|_{1,h}} \gtrsim \|q_h\|_{0,\Omega}, \quad \forall q_h \in Q_h.$$

Proof. Let $\underline{H}_N^1(\Omega) := \{\underline{v} \in \underline{H}^1(\Omega) : \underline{v} = 0 \text{ on } \Gamma_N\}$. Define $\Pi_C : \underline{H}_N^1(\Omega) \mapsto \underline{C}_h^N$ by

$$\begin{cases} \Pi_C \underline{v}(a) = R_h \underline{v}(a), & \forall a \in \mathcal{N}_h, \\ \int_e (\Pi_C \underline{v} - \underline{v}) \cdot \mathbf{n}_e ds = 0, & \forall e \in \mathcal{E}_h, \\ \int_T x \operatorname{div} (\Pi_C \underline{v} - \underline{v}) dT = 0, \quad \int_T y \operatorname{div} (\Pi_C \underline{v} - \underline{v}) dT = 0, & \forall T \in \mathcal{T}_h, \end{cases}$$

where R_h represents the local L^2 -projection given in [19, (A.53)–(A.54)]. It can be verified directly that $(\operatorname{div} \Pi_C \underline{v}, q_h) = (\operatorname{div} \underline{v}, q_h)$ for any $q_h \in Q_h$, and $|\Pi_C \underline{v}|_{1,h} \lesssim |\underline{v}|_{1,h}$. Hence the stability (2.11) is valid [17, Propositions 4.1–4.2]. \square

Lemma 2.11. *For any $\underline{v} \in \underline{V}_{hD}$ and $\underline{z} \in \underline{C}_h^N$, it holds that*

$$(2.12) \quad \sum_{T \in \mathcal{T}_h} \int_T \nabla \underline{v} : \operatorname{curl} \underline{z} dT = 0.$$

Proof. Let subscripts “ \cdot_1 ” and “ \cdot_2 ” represent the components of the vector in the x and y directions, respectively. Integration by parts and direct calculation lead to

$$(2.13) \quad \begin{aligned} \sum_{T \in \mathcal{T}_h} \int_T \nabla \underline{v} : \operatorname{curl} \underline{z} dT &= \sum_{T \in \mathcal{T}_h} \sum_{e \subset \partial T} \int_e (v_1 \nabla z_1 \cdot \mathbf{t}_{T,e} + v_2 \nabla z_2 \cdot \mathbf{t}_{T,e}) ds \\ &= \sum_{T \in \mathcal{T}_h} \sum_{e \subset \partial T} \int_e (\underline{v} \cdot \mathbf{n}_{T,e})(\underline{g}_{T,e} \cdot \mathbf{n}_{T,e}) + (\underline{v} \cdot \mathbf{t}_{T,e})(\underline{g}_{T,e} \cdot \mathbf{t}_{T,e}) ds, \end{aligned}$$

where $\underline{g}_{T,e} := \nabla \underline{z} \cdot \mathbf{t}_{T,e}$, $\mathbf{t}_{T,e}$ is the counter-clockwise unit tangent vector of T on e and $\mathbf{n}_{T,e}$ represents the unit outer normal vector. Notice that $\underline{z}|_e \in (P_1)^2 + \operatorname{span}\{\phi_{T,e} \cdot \mathbf{n}_{T,e}\}$, and $\phi_{T,e}$ is the quadratic bubble function associated with e in T , we derive that $\underline{g}_{T,e} \cdot \mathbf{t}_{T,e}$ is constant on each $e \subset \partial T$. We check the right hand part of (2.13) case by case.

Case 1. For $e \in \mathcal{E}_h^i$ with $T_1 \cap T_2 = e$. Utilizing the continuity of $\underline{v} \cdot \mathbf{n}$, $\mathbf{n}_{T_1,e} = -\mathbf{n}_{T_2,e}$, $\mathbf{t}_{T_1,e} = -\mathbf{t}_{T_2,e}$, and $\underline{g}_{T_1,e} = -\underline{g}_{T_2,e}$ by $\underline{z} \in \underline{H}^1(\Omega)$, we obtain

$$\int_e (\underline{v} \cdot \mathbf{n}_{e,T_1})(\underline{g}_{T_1,e} \cdot \mathbf{n}_{e,T_1}) + \int_e (\underline{v} \cdot \mathbf{n}_{T_2,e})(\underline{g}_{T_2,e} \cdot \mathbf{n}_{T_2,e}) = \int_e \underline{v} \cdot \mathbf{n}_{e,T_1} (\underline{g}_{T_1,e} \cdot \mathbf{n}_{T_1,e} - \underline{g}_{T_1,e} \cdot \mathbf{n}_{T_1,e}) ds = 0.$$

At the same time, utilizing the continuity of $\int_e \underline{v} \cdot \mathbf{t} ds$ across interior edges, and noticing that $\underline{g}_{T_1,e} \cdot \mathbf{t}_{T_1,e} = \underline{g}_{T_2,e} \cdot \mathbf{t}_{T_2,e} = c$, where c represent a constant on e , we have

$$\int_e (\underline{v} \cdot \mathbf{t}_{T_1,e})(\underline{g}_{T_1,e} \cdot \mathbf{t}_{T_1,e}) + \int_e (\underline{v} \cdot \mathbf{t}_{T_2,e})(\underline{g}_{T_2,e} \cdot \mathbf{t}_{T_2,e}) = (\underline{g}_{T_1,e} \cdot \mathbf{t}_{T_1,e}) \left(\int_e \underline{v} \cdot \mathbf{t}_{T_1,e} ds + \int_e \underline{v} \cdot \mathbf{t}_{T_2,e} ds \right) ds = 0.$$

Case 2. For $e \in \Gamma_D$, $\underline{v} \cdot \mathbf{n}_e = \int_e \underline{v} \cdot \mathbf{t}_e ds = 0$, and $\underline{g}_{T,e} \cdot \mathbf{t}_e$ is constant on $e \in T$. Therefore,

$$\int_e (\underline{v} \cdot \mathbf{n}_{T,e})(\underline{g}_{T,e} \cdot \mathbf{n}_{T,e}) + (\underline{v} \cdot \mathbf{t}_{T,e})(\underline{g}_{T,e} \cdot \mathbf{t}_{T,e}) ds = 0, \quad \forall e \in \Gamma_D.$$

Case 3. For $e \in \Gamma_N$, we have $\underline{z}|_e = \underline{0}$ by definition. Hence $\underline{g}_{T,e} = \underline{0}$ for $e \in T$, and

$$\int_e (\underline{v} \cdot \mathbf{n}_{T,e})(\underline{g}_{T,e} \cdot \mathbf{n}_{T,e}) + (\underline{v} \cdot \mathbf{t}_{T,e})(\underline{g}_{T,e} \cdot \mathbf{t}_{T,e}) ds = 0, \quad \forall e \in \Gamma_N.$$

Namely, the right-hand-side of (2.13) equals to zero. The proof is completed. \square

2.3.2. *Proof of Theorem 2.3.* For any $\underline{v} \in \underline{V}_{hD}$, $\epsilon(\underline{v})|_T = (\nabla \underline{v} - \frac{1}{2} \text{rot } \underline{v} \chi)|_T$, where $\chi = \begin{pmatrix} 0 & -1 \\ 1 & 0 \end{pmatrix}$. From (2.11) and $\text{rot } \underline{v} \in Q_h$, there exists some $\underline{z} \in \underline{C}_h^N$, such that

$$\int_{\Omega} \text{div } \underline{z} q d\Omega = \sum_{T \in \mathcal{T}_h} \int_T \text{rot } \underline{v} q dT, \quad \forall q \in Q_h \quad \text{and} \quad |\underline{z}|_{1,h} \lesssim \|\text{rot } \underline{v}\|_{0,\Omega} \lesssim |\underline{v}|_{1,h}.$$

Therefore, $\|\nabla \underline{v} - \text{curl } \underline{z}\|_{0,\Omega} \leq |\underline{v}|_{1,h} + |\underline{z}|_{1,h} \lesssim |\underline{v}|_{1,h}$, and

$$\begin{aligned} \sum_{T \in \mathcal{T}_h} \int_T \epsilon(\underline{v}) : (\nabla \underline{v} - \text{curl } \underline{z}) dT &= \sum_{T \in \mathcal{T}_h} \int_T (\nabla \underline{v} - \frac{1}{2} \text{rot } \underline{v} \chi) : (\nabla \underline{v} - \text{curl } \underline{z}) dT \\ &= \sum_{T \in \mathcal{T}_h} \int_T |\nabla \underline{v}|^2 dT - \frac{1}{2} \sum_{T \in \mathcal{T}_h} \int_T \text{rot } \underline{v} (\text{rot } \underline{v} - \text{div } \underline{z}) dT = \sum_{T \in \mathcal{T}_h} \int_T |\nabla \underline{v}|^2 dT = |\underline{v}|_{1,h}^2. \end{aligned}$$

Finally $(\sum_{T \in \mathcal{T}_h} \int_T |\epsilon(\underline{v})|^2 dT)^{\frac{1}{2}} \geq \frac{\sum_{T \in \mathcal{T}_h} \int_T \epsilon(\underline{v}) : (\nabla \underline{v} - \text{curl } \underline{z}) dT}{\|\nabla \underline{v} - \text{curl } \underline{z}\|_{0,\Omega}} \gtrsim |\underline{v}|_{1,h}$, and the proof is completed.

3. APPLICATION TO STOKES PROBLEMS

3.1. **Application to the Stokes equations.** Consider the stationary Stokes system:

$$(3.1) \quad \begin{cases} -\varepsilon^2 \Delta \underline{u} + \nabla p = \underline{f} & \text{in } \Omega, \\ \text{div } \underline{u} = g & \text{in } \Omega, \\ \underline{u} = 0, & \text{on } \Gamma_D. \end{cases}$$

For simplicity of presentation, we only consider the case of $\partial\Omega = \Gamma_D$ herein. Extensions to other boundary conditions follows directly.

The discretization scheme of (3.1) reads: Find $(\underline{u}_h, p_h) \in \underline{V}_{h0} \times Q_{h*}$, such that

$$(3.2) \quad \begin{cases} \varepsilon^2 (\nabla_h \underline{u}_h, \nabla_h \underline{v}_h) - (\text{div } \underline{v}_h, p_h) = \langle \underline{f}, \underline{v}_h \rangle & \forall \underline{v}_h \in \underline{V}_h, \\ (\text{div } \underline{u}_h, q_h) = \langle g, q_h \rangle & \forall q_h \in Q_h. \end{cases}$$

Based on the discussions in Section 2, Brezzi's conditions can be easily verified, and (3.2) is uniformly well-posed with respect to ε and h .

Theorem 3.1. *Let (\underline{u}, p) and (\underline{u}_h, p_h) be the solutions of (3.1) and (3.2), respectively. The following estimates hold with $0 < r \leq 2$*

$$\begin{aligned} \|\underline{u} - \underline{u}_h\|_{1,h} &\lesssim h^r \|\underline{u}\|_{r+1,\Omega} + h \|\underline{u}\|_{2,\Omega}, \\ \|p - p_h\|_{0,\Omega} &\lesssim h^r \|p\|_{r,\Omega} + \varepsilon^2 (h^r \|\underline{u}\|_{r+1,\Omega} + h \|\underline{u}\|_{2,\Omega}). \end{aligned}$$

Proof. Since the mixed element is inf-sup stable, divergence-free, and $\underline{v}_h \cdot \mathbf{n}$ is continuous, the following estimates are standard [6, 8, 12]:

$$\begin{aligned} |\underline{u} - \underline{u}_h|_{1,h} &\lesssim \inf_{\underline{w}_h \in \underline{V}_h} |\underline{u} - \underline{w}_h|_{1,h} + \sup_{\underline{v}_h \in \underline{Z}_h(0)} \frac{\left| \sum_{e \in \mathcal{E}_h} \varepsilon^2 \int_e (\nabla \underline{u} \cdot \mathbf{n}_e) \cdot \llbracket \underline{v}_h \rrbracket ds \right|}{\varepsilon^2 |\underline{v}_h|_{1,h}}, \\ \|p - p_h\|_{0,\Omega} &\lesssim \varepsilon^2 |\underline{u} - \underline{u}_h|_{1,h} + \inf_{q_h \in Q_h} \|p - q_h\|_{0,\Omega} + \sup_{\underline{v}_h \in \underline{V}_h} \frac{\left| \sum_{e \in \mathcal{E}_h} \varepsilon^2 \int_e (\nabla \underline{u} \cdot \mathbf{n}_e) \cdot \llbracket \underline{v}_h \rrbracket ds \right|}{|\underline{v}_h|_{1,h}}. \end{aligned}$$

The term $\inf_{\underline{w}_h \in \underline{V}_h} |\underline{u} - \underline{w}_h|_{1,h}$ is bounded by the interpolation error. Since $\int_e \underline{v}_h ds$ is continuous across interior edges and vanish on $\partial\Omega$, a standard estimate similar to that of the Crouzeix and Raviart element [11, Lemma 3] leads to

$$(3.3) \quad \left| \sum_{e \in \mathcal{E}_h} \varepsilon^2 \int_e (\nabla \underline{u} \cdot \mathbf{n}_e) \cdot \llbracket \underline{v}_h \rrbracket ds \right| \lesssim \varepsilon^2 h |\underline{u}|_{2,\Omega} |\underline{v}_h|_{1,h}.$$

Hence we derive

$$|\underline{u} - \underline{u}_h|_{1,h} \lesssim h^r |\underline{u}|_{r+1,\Omega} + h |\underline{u}|_{2,\Omega} \quad \text{with } 0 < r \leq 2.$$

The above estimates together with $\inf_{q_h \in Q_h} \|p - q_h\|_{0,\Omega} \lesssim h^r |p|_{r,\Omega}$ lead to that

$$\|p - p_h\|_{0,\Omega} \lesssim h^r |p|_{r,\Omega} + \varepsilon^2 (h^r |\underline{u}|_{r+1,\Omega} + h |\underline{u}|_{2,\Omega}) \quad \text{with } 0 < r \leq 2.$$

The proof is completed. \square

3.2. Application to the Darcy–Stokes–Brinkman equations. Consider the Darcy–Stokes–Brinkman equations:

$$(3.4) \quad \begin{cases} -\varepsilon^2 \Delta \underline{u} + \underline{u} + \nabla p = \underline{f} & \text{in } \Omega, \\ \operatorname{div} \underline{u} = g & \text{in } \Omega, \\ \underline{u} \cdot \mathbf{n} = 0, \quad \varepsilon \underline{u} \cdot \mathbf{t} = 0 & \text{on } \partial\Omega, \end{cases}$$

where $\varepsilon \in (0, 1]$ is a parameter. When ε is not too small and $g = 0$, it is a Stokes problem with an additional lower order term. When $\varepsilon = 0$, the first equation becomes the Darcy's law for porous medium flow. Most classic mixed elements fail to converge uniformly with respect to ε when applied to (3.4) [33].

The discretization scheme of (3.4) reads: Find $(\underline{u}_h, p_h) \in \underline{V}_{h0} \times Q_{h*}$, such that

$$(3.5) \quad \begin{cases} \varepsilon^2 (\nabla_h \underline{u}_h, \nabla_h \underline{v}_h) + (\underline{u}_h, \underline{v}_h) - (\operatorname{div} \underline{v}_h, p_h) = \langle \underline{f}, \underline{v}_h \rangle & \forall \underline{v}_h \in \underline{V}_h, \\ (\operatorname{div} \underline{u}_h, q_h) = \langle g, q_h \rangle & \forall q_h \in Q_h. \end{cases}$$

Since the finite element pair is stable and conservative, Brezzi's conditions can be easily verified for (3.5), and it is uniformly well-posed with respect to ε and h , provided $\int_{\Omega} g d\Omega = 0$. Robust convergence can be obtained both for smooth continuous solutions and for the case that the effect of the ε -dependent boundary layers is taken into account later.

Theorem 3.2. *If $\underline{u} \in \underline{H}^{r+1}(\Omega) \cap \underline{H}_0^1(\Omega)$ and $p \in H^r(\Omega) \cap L_0^2(\Omega)$ with $0 < r \leq 2$, then*

$$(3.6) \quad \|\operatorname{div} \underline{u} - \operatorname{div} \underline{u}_h\|_{0,\Omega} \lesssim h^r |\underline{u}|_{r+1,\Omega},$$

$$(3.7) \quad \|\underline{u} - \underline{u}_h\|_{0,\Omega} + \varepsilon |\underline{u} - \underline{u}_h|_{1,h} \lesssim h^r (\varepsilon + h) |\underline{u}|_{r+1,\Omega} + \varepsilon h |\underline{u}|_{2,\Omega},$$

$$(3.8) \quad \|p - p_h\|_{0,\Omega} \lesssim h^r |p|_{r,\Omega} + h^r (\varepsilon + h) |\underline{u}|_{r+1,\Omega} + \varepsilon h |\underline{u}|_{2,\Omega}.$$

Proof. Evidently, $\operatorname{div} \underline{u}_h = P_{Q_{h^*}}(\operatorname{div} \underline{u})$, where $P_{Q_{h^*}}$ represents the L^2 -projection into Q_{h^*} . Therefore, the first inequality (3.6) follows from the estimation of the L^2 -projection. For this conservative pair, the following estimates are standard (see, e.g., [8] and [33]),

$$(3.9) \quad \|\underline{u} - \underline{u}_h\|_{0,\Omega} + \varepsilon |\underline{u} - \underline{u}_h|_{1,h} \lesssim$$

$$\inf_{\underline{w}_h \in \underline{V}_h} (\|\underline{u} - \underline{w}_h\|_{0,\Omega} + \varepsilon |\underline{u} - \underline{w}_h|_{1,h}) + \sup_{\underline{v}_h \in \underline{Z}_h(0)} \frac{\left| \sum_{e \in \mathcal{E}_h} \varepsilon^2 \int_e (\nabla \underline{u} \cdot \mathbf{n}_e) \cdot \llbracket \underline{v}_h \rrbracket ds \right|}{\varepsilon |\underline{v}_h|_{1,h}},$$

$$(3.10) \quad \|p - p_h\|_{0,\Omega} \lesssim \|\underline{u} - \underline{u}_h\|_{0,\Omega} + \varepsilon |\underline{u} - \underline{u}_h|_{1,h}$$

$$+ \inf_{q_h \in Q_h} \|p - q_h\|_{0,\Omega} + \sup_{\underline{v}_h \in \underline{V}_h} \frac{\left| \sum_{e \in \mathcal{E}_h} \varepsilon^2 \int_e (\nabla \underline{u} \cdot \mathbf{n}_e) \cdot \llbracket \underline{v}_h \rrbracket ds \right|}{\varepsilon |\underline{v}_h|_{1,h}}.$$

Hence (3.7) and (3.8) are derived in a similar way as those in Theorem 3.1. \square

As is mentioned in [33], it may happen that $|\underline{u}|_{2,\Omega}$ and $|\underline{u}|_{3,\Omega}$ blow up as ε tends to 0. In this case, the convergence estimates given in Theorem 3.2 will deteriorate, especially when the solution of (3.4) has boundary layers. To derive a uniform convergence analysis of the discrete solutions, we assume that Ω is a convex polygon. Let $\{a_j := (x_j, y_j)\}$ denote the set of corner nodes of Ω . Define

$$H_+^1(\Omega) := \left\{ g \in H^1(\Omega) \cap L_0^2(\Omega) : \int_{\Omega} \frac{|g(x, y)|}{(x - x_j)^2 + (y - y_j)^2} d\Omega < \infty, j = 1, 2, \dots, l \right\},$$

with associated norm

$$\|g\|_{1,+}^2 := \|g\|_{1,\Omega}^2 + \sum_{j=1}^l \int_{\Omega} \frac{|g(x, y)|}{(x - x_j)^2 + (y - y_j)^2} d\Omega.$$

Let (\underline{u}^0, p^0) solves (3.4) in the case of $\varepsilon = 0$. Then it is proved in [33] that

$$(3.11) \quad \begin{aligned} \varepsilon^2 \|\underline{u}\|_{2,\Omega} + \varepsilon \|\underline{u}\|_{1,\Omega} + \|\underline{u} - \underline{u}^0\|_{0,\Omega} + \|p - p^0\|_{1,\Omega} + \varepsilon^{\frac{1}{2}} \|\underline{u}^0\|_{1,\Omega} + \varepsilon^{\frac{1}{2}} \|p^0\|_{1,\Omega} \\ \lesssim \varepsilon^{\frac{1}{2}} (\|\underline{f}\|_{\operatorname{rot}} + \|g\|_{1,+}), \end{aligned}$$

where $\|\cdot\|_{\operatorname{rot}} := \|\cdot\|_{0,\Omega} + \|\operatorname{rot}(\cdot)\|_{0,\Omega}$ is the norm defined in $\underline{H}(\operatorname{rot}, \Omega)$. Following the technique in [33], we can obtain the following uniform convergence estimate.

Theorem 3.3. *Let (\underline{u}, p) be the exact solution of (3.4) and (\underline{u}_h, p_h) be its approximation in $\underline{V}_{h0} \times Q_{h*}$. If $f \in \underline{H}(\text{rot}, \Omega)$ and $g \in H_+^1(\Omega)$, then*

$$(3.12) \quad \|\text{div } \underline{u} - \text{div } \underline{u}_h\| \lesssim h \|g\|_{1,\Omega},$$

$$(3.13) \quad \|\underline{u} - \underline{u}_h\|_{0,\Omega} + \varepsilon |\underline{u} - \underline{u}_h|_{1,h} \lesssim h^{\frac{1}{2}} (\|f\|_{\text{rot}} + \|g\|_{1,+}),$$

$$(3.14) \quad \|p - p_h\|_{0,\Omega} \lesssim h^{\frac{1}{2}} (\|f\|_{\text{rot}} + \|g\|_{1,+}).$$

Proof. The first estimate is direct since $\text{div } \underline{u} = g$. To obtain the second inequality, we first analyze the interpolation error. By (2.2), (2.3), and (3.11), we have

$$(3.15) \quad \begin{aligned} \|\underline{u} - \Pi_h \underline{u}\|_{0,\Omega} &\leq \|(\mathbf{I} - \Pi_h)(\underline{u} - \underline{u}^0)\|_{0,\Omega} + \|\underline{u}^0 - \Pi_h \underline{u}^0\|_{0,\Omega} \\ &\lesssim h^{\frac{1}{2}} (\|\underline{u} - \underline{u}^0\|_{0,\Omega}^{\frac{1}{2}} \|\underline{u} - \underline{u}^0\|_{1,\Omega}^{\frac{1}{2}} + h^{\frac{1}{2}} \|\underline{u}^0\|_{1,\Omega}) \lesssim h^{\frac{1}{2}} (\|f\|_{\text{rot}} + \|g\|_{1,+}). \end{aligned}$$

At the same time,

$$(3.16) \quad \varepsilon |\underline{u} - \Pi_h \underline{u}|_{1,h} \lesssim \varepsilon |\underline{u}|_{1,\Omega}^{\frac{1}{2}} |\underline{u} - \Pi_h \underline{u}|_{1,h}^{\frac{1}{2}} \lesssim \varepsilon h^{\frac{1}{2}} |\underline{u}|_{1,\Omega}^{\frac{1}{2}} |\underline{u}|_{2,\Omega}^{\frac{1}{2}} \lesssim h^{\frac{1}{2}} (\|f\|_{\text{rot}} + \|g\|_{1,+}),$$

where we utilize $\varepsilon |\underline{u}|_{1,\Omega}^{\frac{1}{2}} |\underline{u}|_{2,\Omega}^{\frac{1}{2}} \lesssim \varepsilon^{\frac{1}{2}} |\underline{u}|_{1,\Omega} + \varepsilon^{\frac{3}{2}} |\underline{u}|_{2,\Omega} \lesssim \|f\|_{\text{rot}} + \|g\|_{1,+}$.

By the continuity of $\underline{v}_h \cdot \mathbf{n}_e$ and $\int_e \underline{v}_h \cdot \mathbf{t}_e ds$, a standard estimate (see, e.g., [33, Lemma 5.1]) yields $\sum_{e \in \mathcal{E}_h} \varepsilon^2 \int_e (\nabla \underline{u} \cdot \mathbf{n}_e) \cdot \llbracket \underline{v}_h \rrbracket ds \lesssim \varepsilon^2 h^{\frac{1}{2}} |\underline{u}|_{1,\Omega}^{\frac{1}{2}} |\underline{u}|_{2,\Omega}^{\frac{1}{2}} |\underline{v}_h|_{1,h}$. Then we derive

$$(3.17) \quad \frac{\left| \sum_{e \in \mathcal{E}_h} \varepsilon^2 \int_e (\nabla \underline{u} \cdot \mathbf{n}_e) \cdot \llbracket \underline{v}_h \rrbracket ds \right|}{\varepsilon |\underline{v}_h|_{1,h}} \lesssim \varepsilon h^{\frac{1}{2}} |\underline{u}|_{1,\Omega}^{\frac{1}{2}} |\underline{u}|_{2,\Omega}^{\frac{1}{2}} \lesssim h^{\frac{1}{2}} (\|f\|_{\text{rot}} + \|g\|_{1,+}).$$

A combination of (3.9), (3.15), (3.16), and (3.17) leads to

$$(3.18) \quad \|\underline{u} - \underline{u}_h\|_{0,\Omega} + \varepsilon |\underline{u} - \underline{u}_h|_{1,h} \lesssim h^{\frac{1}{2}} (\|f\|_{\text{rot}} + \|g\|_{1,+}).$$

Again from (3.11) and notice that $\varepsilon < 1$, we have

$$(3.19) \quad \|p - \Pi_{Q_h} p\|_{0,\Omega} \lesssim h |p|_{1,\Omega} \lesssim h |p - p^0|_{1,\Omega} + h |p^0|_{1,\Omega} \lesssim h (\|f\|_{\text{rot}} + \|g\|_{1,+}).$$

Hence, by (3.10), (3.18), and (3.19), the last estimate (3.14) is derived. \square

4. NUMERICAL EXPERIMENTS

In this section, we carry out numerical experiments to validate the theory and illustrate the capacity of the newly proposed element pair. Examples are given as illustrations from different perspectives.

- Examples 1 and 2 test the method with the Stokes problem, especially its robustness with respect to the Reynolds' number and to the triangulations;
- Examples 3 and 4 test the method with the Darcy–Stokes–Brinkman equation, especially the robustness with respect to the the small parameter, for smooth solutions as well as solutions with sharp layers;
- Examples 5 and 6 test the method with the incompressible Navier–Stokes equation, regarding evolutionary and steady states.

Three kinds of $P_2 - P_1$ pairs are involved in the experiments, namely,

TH: the Taylor-Hood element pair with continuous P_2 functions for the velocity space and continuous P_1 functions for the pressure space;

SV: the Scott-Vogelius element pair with continuous P_2 functions for the velocity space and discontinuous P_1 functions for the pressure space;

NPP: the newly proposed $P_2 - P_1$ element pair.

All simulations are performed on uniformly refined grids. For the SV pair, an additional barycentric refinement is applied on each grid to guarantee the stability.

Example 1. This example was suggested in [29] to illustrate the non-pressure-robustness of classical elements. Let $\Omega = (0, 1)^2$. Consider the Stokes equations (3.1) with $\varepsilon^2 = 1$, $g = 0$, and $\underline{f} = (0, Ra(1 - y + 3y^2))^T$, where $Ra > 0$ represents a parameter. No-slip boundary conditions are imposed on $\partial\Omega$. The exact solution pair is $\underline{u} = \underline{0}$ and $p = Ra(y^3 - \frac{y^2}{2} + y - \frac{7}{12})$.

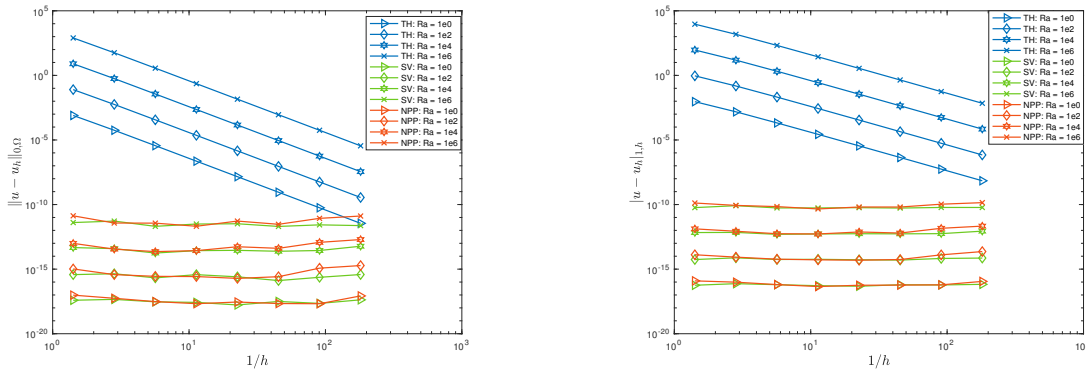


FIGURE 3. Example 1: Velocity errors in the no-flow Stokes equations by the TH, SV, and NPP pairs.

For the continuous problem, different values of Ra result in different exact pressures and the same exact velocity vector. As is shown in Figure 3, for both the SV and NPP pairs, the numerical velocities are very close to zero for different values of Ra . However, for the TH pair, the discrete velocity is far from zero, even when $Ra = 1$. It demonstrates the advantage of pressure-robust pairs especially for problems with large pressures.

Example 2. This example was also introduced in [29]. Let $\Omega = (0, 4) \times (0, 2) \setminus [2, 4] \times [0, 1]$. Consider a flow with Coriolis forces with the following form

$$\begin{cases} -\varepsilon^2 \Delta \underline{u} + \nabla p + 2 \underline{w} \times \underline{u} = \underline{f} & \text{in } \Omega, \\ \operatorname{div} \underline{u} = 0 & \text{in } \Omega, \end{cases}$$

where $\underline{w} = (0, 0, w)^T$ is a constant angular velocity vector. Changing the magnitude w will change only the exact pressure, and not the true velocity solution. Dirichlet boundary conditions are imposed on $\partial\Omega$; see Figure 4 (Left). The computed domain and initial unstructured grid are depicted in Figure 4. Simulations were performed with $\varepsilon^2 = 0.01$, while $w = 100$ or $w = 1000$.

Computed velocities (speed) with $w = 100$ and $w = 1000$ are depicted in Figures 5 and 6, respectively. The solutions computed with the SV and NPP pairs are considerably more accurate compared with the TH pair. Moreover, when $w = 1000$, the advantages of divergence-free elements are more obvious on the third level grid.

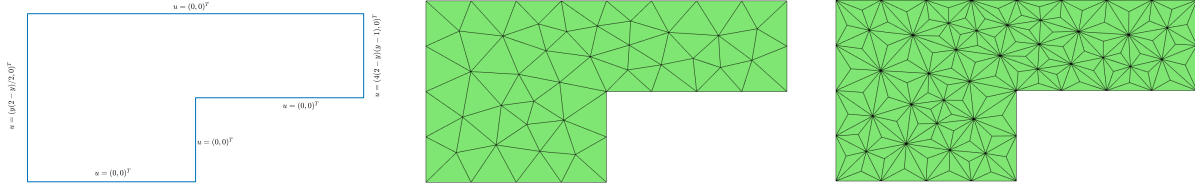


FIGURE 4. Example 2: Forward facing step domain, unstructured mesh (level 1), and unstructured barycentric mesh for the SV pair (level 1).

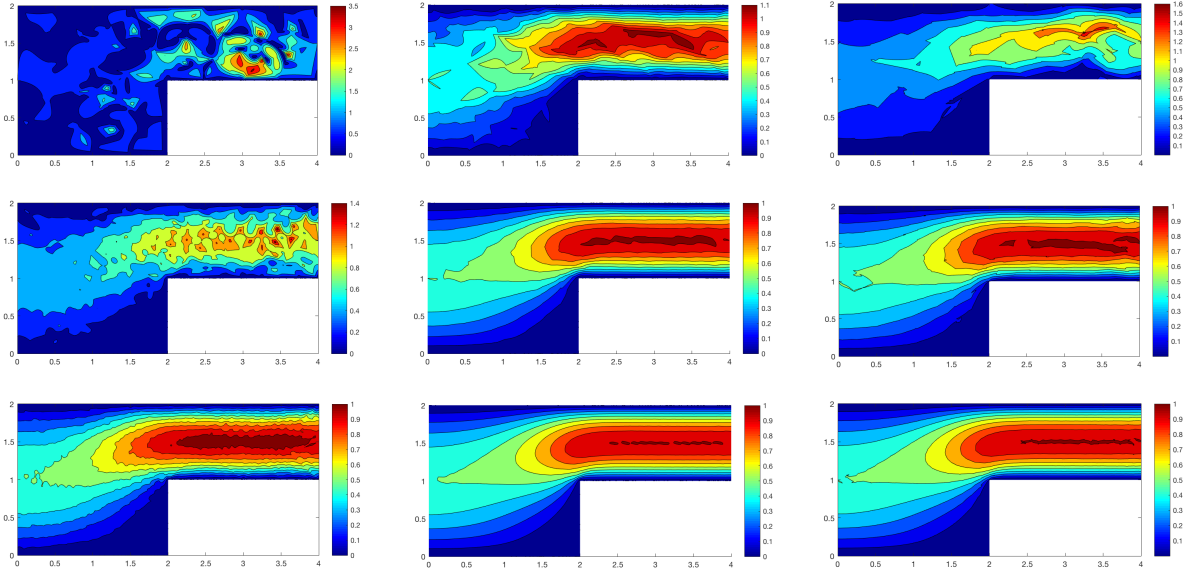


FIGURE 5. Example 2 ($w = 100$ and $\varepsilon^2 = 0.01$): Speed obtained by the TH pair (left column), the SV pair (middle column), and the NPP pair (right column); rows 1 – 3 are results on meshes 1–3.

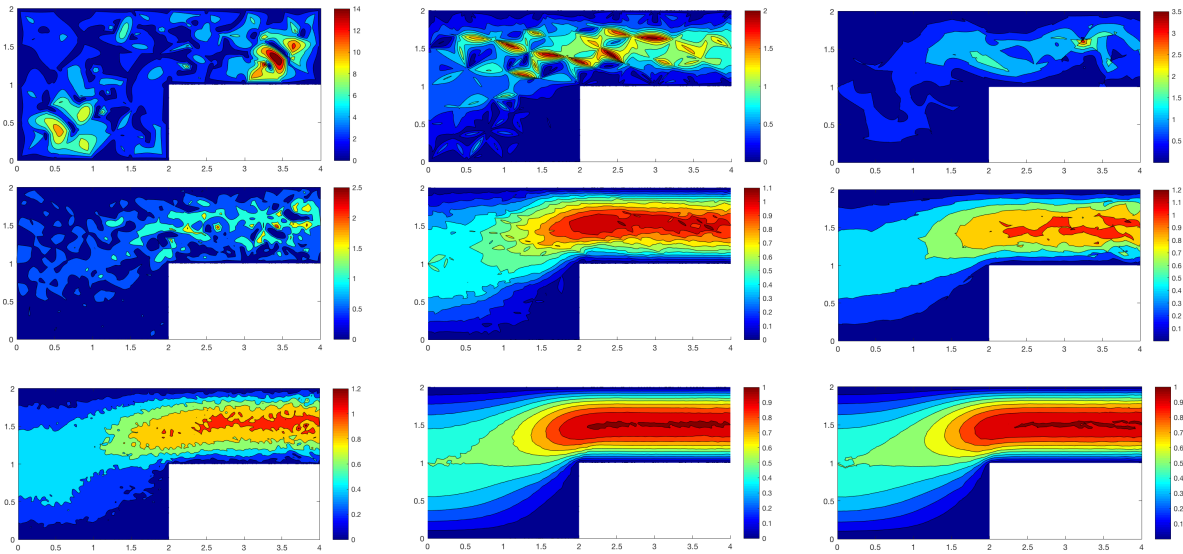


FIGURE 6. Example 2 ($w = 1000$ and $\varepsilon^2 = 0.01$): Speed obtained by the TH pair (left column), the SV (middle column), and the NPP pair (right column); rows 1 – 3 are results on meshes 1 – 3.

To compare the mesh dependence of these three pairs, we apply them on a structured mesh without additional barycentric refinement (Figure 7). This type of meshes are generally considered of good quality and commonly used. As is shown in Figure 8, the simulation by the SV pair turns out to be not reliable on the grid, while the NPP pair plays fine.



FIGURE 7. Forward facing step domain and structured non-barycentric mesh.

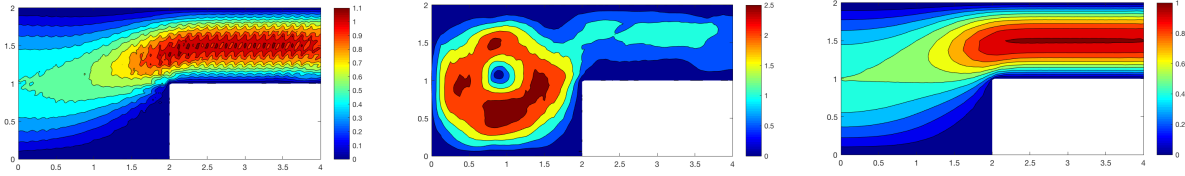


FIGURE 8. Example 2 ($w = 100$ and $\varepsilon^2 = 0.01$): Simulation by the SV pair (middle) is not as good as the TH pair (left) nor the NPP pair (right) on non-barycentric mesh.

Example 3. Let $\Omega = (0, 1)^2$. We consider the Darcy–Stokes–Brinkman problem with

$$\underline{u} = \text{curl}(\sin^2(\pi x)\sin^2(\pi y)) = \pi \begin{pmatrix} \sin^2(\pi x)\sin(2\pi y) \\ -\sin^2(\pi y)\sin(2\pi x) \end{pmatrix}; \quad p = \frac{2}{\pi} - \sin(\pi x).$$

The force \underline{f} is computed by $\underline{f} = -\varepsilon^2 \Delta \underline{u} + \underline{u} + \nabla p$, and $g = \text{div} \underline{u} = 0$. The solution is smooth and independent of ε . We start from an unstructured initial triangular grid, and it is successively refined to maintain the quality of grids.

In Figure 9, we draw convergence curves of the NPP pair with different values of ε , where curves represents actual error declines while triangles illustrates theoretic convergence rates correspondingly. As is shown, when $0 < \varepsilon < 1$, errors in L^2 -norm are of $O(h^2)$ order and errors in H^1 -norm are of $O(h)$ order. In the limiting case of $\varepsilon = 0$, the L^2 -norm error reaches $O(h^3)$ order and H^1 -norm error reaches $O(h^2)$ order, which is due to the fact that \underline{V}_{h0} is a conforming subspace of $\underline{H}(\text{div}, \Omega)$.

In Figure 10, we present the errors in the norm $||| \cdot |||_{\varepsilon,h}$ by the TH pair and the NPP pair when $\varepsilon = 2^{-8}$. Here $||| \underline{v} |||_{\varepsilon,h} := \varepsilon^2 \|\underline{v}\|_{1,h}^2 + \|\underline{v}\|_{0,\Omega} + \|\text{div} \underline{v}\|_{0,\Omega}^2$ is the commonly used norm which combines the Stokes and Darcy problems. Although the convergence rate of the NPP pair is one order lower than that of the TH pair, the error of the former is smaller (several magnitudes) than that of the latter in the figure where millions of DOFs have been used on the finest grid. For the NPP pair, the associated energy error of velocity is close to 10^{-3} , while for the TH pair, it does not reach an error of 10^{-3} even on the eighth level mesh. However, as remarked in the figure, the degrees of freedom of the TH pair (on the eighth level mesh) is over 500 times more than the NPP pair (on the third level mesh).

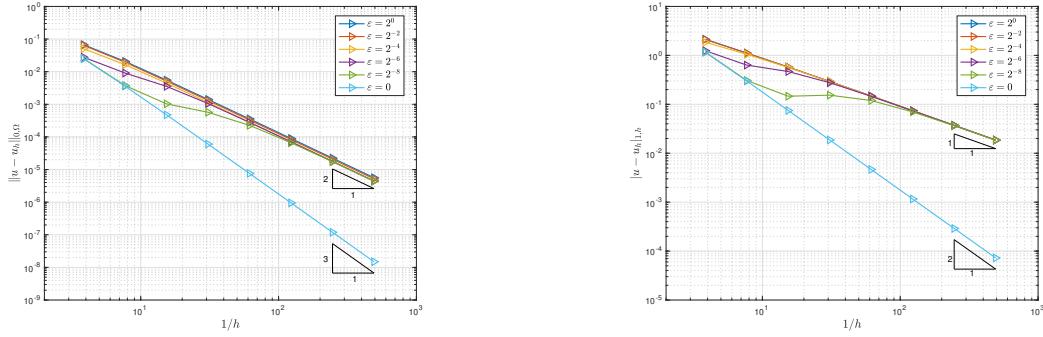


FIGURE 9. Example 3: Velocity errors in the L^2 -norm (left) and in the H^1 -norm (right) by the NPP method.

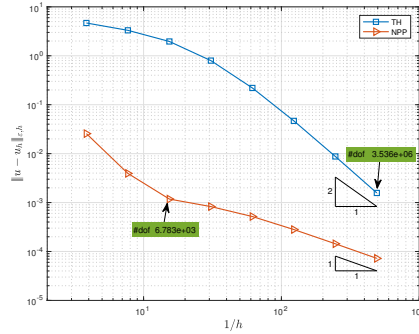


FIGURE 10. Example 3: Errors of velocity in the energy norm by the NPP pair and the TH pair when $\varepsilon = 2^{-8}$.

Example 4. Let $\Omega = (0, 1)^2$. Consider the Darcy–Stokes–Brinkman problem with

$$\underline{u} = \varepsilon \text{curl} \left(e^{-\frac{xy}{\varepsilon}} \right) = \begin{pmatrix} -xe^{-\frac{xy}{\varepsilon}} \\ ye^{-\frac{xy}{\varepsilon}} \end{pmatrix}; \quad p = -\varepsilon e^{-\frac{x}{\varepsilon}}.$$

The boundary layers of the exact velocity \underline{u} are shown in Figure 11.

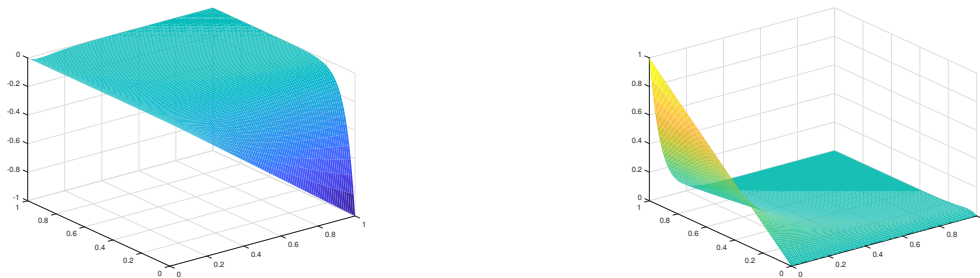


FIGURE 11. Example 4: x -component (left) and y -component (right) of the exact velocity with boundary layers when $\varepsilon = 2^{-4}$.

From Table 1, the convergence rate of velocity is approximately one if ε is sufficiently large, and it decreases to half an order as ε approaches zero, which is consistent with the analysis in Theorem 3.3. From Table 2, the discrete pressure exhibits $O(h)$ order of convergence, higher than the theoretical estimation $O(h^{1/2})$ order.

TABLE 1. Example 4 (with boundary layers): Errors of velocity in the energy norm by the NPP element.

$\varepsilon \setminus h$	2.599E-1	1.300E-01	6.498E-02	3.249E-02	1.625E-02	Rate
2^{-4}	2.998E-02	1.147E-02	4.958E-03	2.430E-03	1.228E-03	1.15
2^{-6}	6.589E-02	3.000E-02	1.159E-02	4.228E-03	1.753E-03	1.33
2^{-8}	1.061E-01	6.246E-02	3.238E-02	1.438E-02	5.504E-03	1.07
2^{-10}	1.171E-01	7.906E-02	5.147E-02	3.061E-02	1.601E-02	0.71
2^{-12}	1.234E-01	8.455E-02	5.688E-02	3.848E-02	2.529E-02	0.57

TABLE 2. Example 4 (with boundary layers): Errors of pressure in the L^2 -norm by the NPP element.

$\varepsilon \setminus h$	2.599E-1	1.300E-01	6.498E-02	3.249E-02	1.625E-02	Rate
2^{-4}	2.260E-03	8.080E-04	2.884E-04	1.211E-04	5.702E-05	1.34
2^{-6}	2.779E-03	7.880E-04	2.696E-04	9.042E-05	2.938E-05	1.63
2^{-8}	6.283E-03	2.044E-03	5.366E-04	1.273E-04	3.448E-05	1.90
2^{-10}	6.730E-03	3.056E-03	1.339E-03	4.607E-04	1.235E-04	1.43
2^{-12}	6.710E-03	3.044E-03	1.440E-03	7.024E-04	3.216E-04	1.09

Example 5. Let $\Omega = (0, 1)^2$. Consider the incompressible Navier–Stokes equations

$$(4.1) \quad \begin{cases} \partial_t \underline{u} - \varepsilon^2 \Delta \underline{u} + (\underline{u} \cdot \nabla) \underline{u} + \nabla p = \underline{f} & \text{in } \Omega, \\ \operatorname{div} \underline{u} = 0 & \text{in } \Omega, \end{cases}$$

with prescribed solution

$$\underline{u}(x, y, t) = \begin{pmatrix} \sin(1-x) \sin(y+t) \\ -\cos(1-x) \cos(y+t) \end{pmatrix}; \quad p = -\cos(1-x) \sin(y+t).$$

In this example, the Crank–Nicolson scheme is used for time discretization, and the Newton linearization is adopted to handle the nonlinear term. To isolate the spatial error, let the time-step $dt = 10^{-3}$ and the final time be 10^{-2} . Unstructured subdivisions illustrated in Example 2 are utilized.

As is depicted in Table 3 with $\varepsilon^2 = 10^{-6}$, solutions by the TH pair converge with $O(h^{3/2})$ order in the L^2 -norm, and by the SV pair they converge with $O(h^2)$ order. It is analyzed in [32] that the TH pair loses order mainly because it is not pressure-robust, while the suboptimal result of the SV pair is due to additional error sources arising from the nonlinear term. The NPP pair exhibits a convergence rate of $O(h^2)$ order which is consistent with its theoretical analysis, and it gives even a more accurate approximation than the SV pair in this case.

TABLE 3. Example 5 ($\varepsilon^2 = 10^{-6}$): Errors of velocity in the L^2 -norm.

h	TH		SV		NPP	
	$\ (\underline{u} - \underline{u}_h)(T)\ _{0,\Omega}$	Rate	$\ (\underline{u} - \underline{u}_h)(T)\ _{0,\Omega}$	Rate	$\ (\underline{u} - \underline{u}_h)(T)\ _{0,\Omega}$	Rate
2.599E-01	1.746E-04	–	1.031E-04	–	7.128E-05	–
1.300E-01	6.006E-05	1.54	1.362E-05	2.92	9.407E-06	2.92
6.498E-02	2.158E-05	1.48	1.989E-06	2.78	1.377E-06	2.77
3.249E-02	7.583E-06	1.51	3.561E-07	2.48	2.488E-07	2.47
1.625E-02	2.524E-06	1.59	7.790E-08	2.19	5.455E-08	2.19

Example 6. Let $\Omega = (0, 1)^2$ be a square domain. Consider the Navier–Stokes equations (4.1) with boundary conditions $\underline{u} = (-1, 0)^T$ on the side $y = 1$ and $\underline{u} = (0, 0)^T$ on the other three sides. Take the viscosity as $\varepsilon^2 = 10^{-3}$.

The backward-Euler time-stepping scheme and the Picard iteration are adopted for this example. Set the time step to be $dt = 0.1$. Consider a long time simulation with the final time equals 90 to derive a steady solution. Indeed, as the solution is steady, the choice of time scheme has little influence on the accuracy of the final solution. Referenced data in a benchmark work [9] are involved to make a reliable comparison, where the solutions are derived on a rather fine mesh, i.e., 1024×1024 rectangular subdivision of domain Ω . We wish to see whether major features of the steady-state flow can be captured on a coarse mesh with $43 \times 43 \times 2$ cells.

Isolines of the streamfunction, vorticity, and pressure fields are displayed in Figures 12, 13, and 14, respectively. Compared with the TH pair, the shapes of contour maps derived by the NPP pair are closer to the reference solution. Specially, the colormap of pressure obtained by the NPP pair and the TH pair are quite different; note the difference between the sidebars. By the values given in [9, Table 1], the NPP pair method gives more accurate approximation of pressure than the TH pair does.

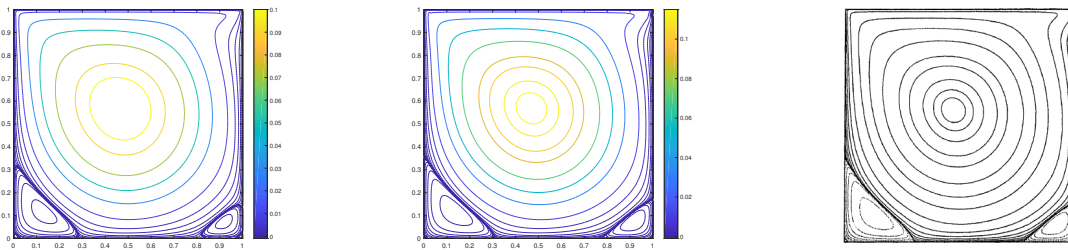


FIGURE 12. Example 6 (streamfunction): Isolines given by the NPP pair (middle) is closer to the reference solution in [9] (right) than the TH pair (left).

The velocity along the centerlines of the cavity is also an important quantity of concern. We can see, from Figure 15, that the results computed by the NPP pair are in better agreement with the reference results in Ref. [9] than the TH pair.

Moreover, the extremes of the streamfunction and the vorticity are depicted in Tables 4 and 5, respectively. Both of them indicate that the NPP pair gives closer results to the benchmark reference results.

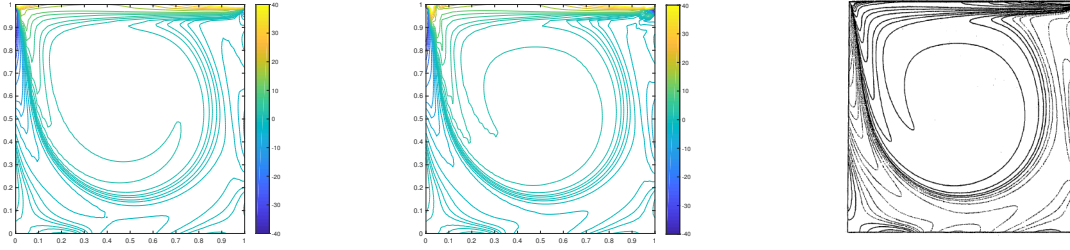


FIGURE 13. Example 6 (vorticity): Isolines derived by the NPP pair (middle) is closer to the reference solution in [9] (right) than the TH pair (left).

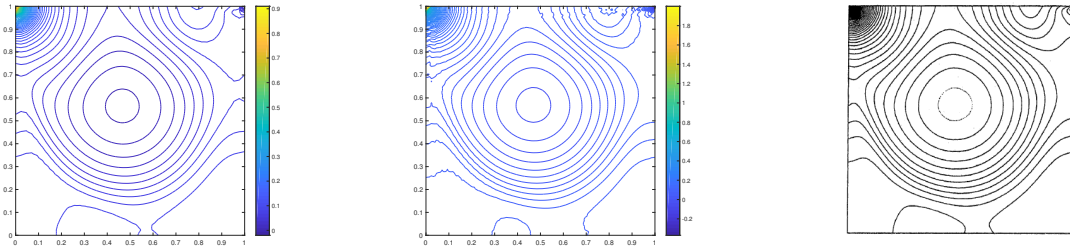


FIGURE 14. Example 6 (pressure): The extreme values of the pressure by the TH pair (left) is notably different with these by the NPP pair (middle), and the latter is closer to the reference values given in [9](right).

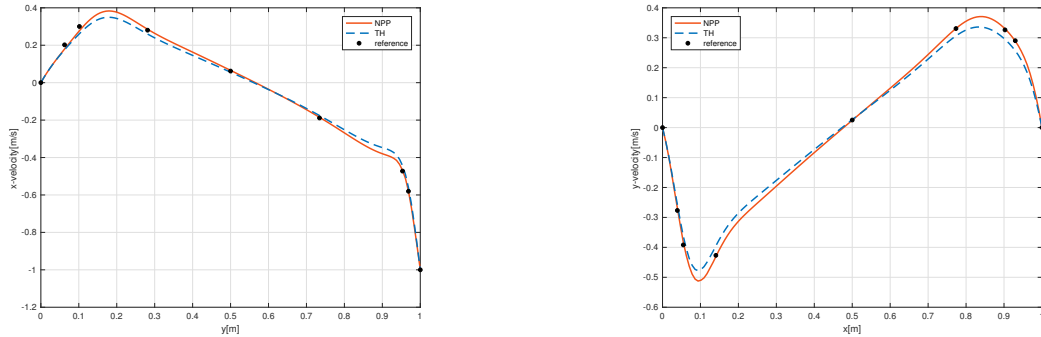


FIGURE 15. Example 6 (velocity profile): x -velocity through the vertical centerline $x = 0.5$ (left), and y -velocity through the horizontal centerline $y = 0.5$ (right).

TABLE 4. Example 6 (streamfunction): Values on the primary and the lower-left secondary vortices.

Scheme	Mesh	Primary	x	y	Secondary	x	y
TH	43×43	1.0862E-01	0.4688	0.5703	-1.3882E-03	0.1328	0.1094
NPP	43×43	1.1733E-01	0.4688	0.5703	-1.6221E-03	0.1406	0.1094
Ref.	1024×1024	1.1892E-01	0.4688	0.5654	-1.7292E-03	0.1367	0.1123

TABLE 5. Example 6 (vorticity): Values on the primary and the lower-left secondary vortices.

Scheme	Mesh	Primary	x	y	Secondary	x	y
TH	43×43	1.8976E+00	0.4688	0.5703	-9.1294E-01	0.1328	0.1094
NPP	43×43	2.0615E+00	0.4688	0.5703	-9.8718E-01	0.1406	0.1094
Ref.	1024×1024	2.0674E+00	0.4688	0.5654	-1.1120E+00	0.1367	0.1123

APPENDIX A. DIMENSION OF THE LOCAL SPACE $\ker(\operatorname{div}, \underline{V}_{h0}(M))$

This appendix is devoted to analyze the basis functions of $\ker(\operatorname{div}, \underline{V}_{h0}(M))$ defined on a macroelement M . Lemma 2.7 is proved at the end of this section.

A.1. Local structure of divergence-free functions. Let T be a triangle with nodes $\{a_i, a_j, a_k\}$ and edges $\{e_i, e_j, e_k\}$. Denote \mathbf{n}_{T,e_l} as a unit outward vector normal to e_l and \mathbf{t}_{T,e_l} as a unit tangential vector of e_l such that $\mathbf{n}_{T,e_l} \times \mathbf{t}_{T,e_l} > 0$, where $l \in \{i, j, k\}$. Denote the lengths of edges by $\{l_i, l_j, l_k\}$, and the area of T by S .



FIGURE 16. Degrees of freedom vanish on dotted edges.

Denote

$$(A.1) \quad \underline{W}_{T,e_j e_k} := \left\{ \underline{v} \in (P_2(T))^2 : \operatorname{div} \underline{v} = 0, \int_{e_i} \underline{v} \cdot \mathbf{t}_{e_i} = 0, \int_{e_i} \underline{v} \cdot \mathbf{n}_{e_i} q = 0, \forall q \in P_2(e_i) \right\},$$

namely, $\underline{W}_{T,e_j e_k}$ consists of quadratic polynomials that are divergence-free and all nodal parameters associated with e_i equal to zero. Denote

$$(A.2) \quad \underline{W}_{T,e_j e_k}^n := \left\{ \underline{v} \in \underline{W}_{T,e_j e_k} : \int_{e_j} \underline{v} \cdot \mathbf{n}_{e_j} = \int_{e_k} \underline{v} \cdot \mathbf{n}_{e_k} = 0 \right\}$$

and

$$(A.3) \quad \underline{W}_{T,e_k} := \underline{W}_{T,e_j e_k} \cap \underline{W}_{T,e_k e_i}.$$

Direct calculation leads to the following results.

Lemma A.1. $\dim(\underline{W}_{T,e_k}) = 1$, $\dim(\underline{W}_{T,e_j e_k}^n) = 4$, and $\dim(\underline{W}_{T,e_j e_k}) = 5$.

A set of basis functions can be constructed explicitly for the local spaces. Recall that $\underline{\varphi}_{\mathbf{n}_{T,e_l},0}$, $\underline{\varphi}_{\mathbf{n}_{T,e_l},1}$, $\underline{\varphi}_{\mathbf{n}_{T,e_l},2}$, and $\underline{\varphi}_{\mathbf{t}_{T,e_l},0}$ represent the basis functions on e_l ; $l \in \{i, j, k\}$. Let

$$\begin{aligned}\underline{w}_{T,e_j} &= \frac{2S}{3l_j^2} \underline{\varphi}_{\mathbf{n}_{T,e_j},1} - \underline{\varphi}_{\mathbf{t}_{T,e_j},0}, & \underline{w}_{T,e_j,e_k} &= -\frac{1}{3l_j} \underline{\varphi}_{\mathbf{n}_{T,e_j},1} + \frac{1}{10l_j} \underline{\varphi}_{\mathbf{n}_{T,e_j},2} - \frac{2}{3l_k} \underline{\varphi}_{\mathbf{n}_{T,e_k},1}, \\ \underline{w}_{T,e_k} &= -\frac{2S}{3l_k^2} \underline{\varphi}_{\mathbf{n}_{T,e_k},1} + \underline{\varphi}_{\mathbf{t}_{T,e_k},0}, & \underline{w}_{T,e_k,e_j} &= -\frac{2}{3l_j} \underline{\varphi}_{\mathbf{n}_{T,e_j},1} - \frac{1}{3l_k} \underline{\varphi}_{\mathbf{n}_{T,e_k},1} - \frac{1}{10l_k} \underline{\varphi}_{\mathbf{n}_{T,e_k},2}, \\ \underline{w}_{T,a_i} &= -\frac{1}{l_j} \underline{\varphi}_{\mathbf{n}_{T,e_j},0} + \frac{-l_i^2 l_j^2 + 2l_i^2 l_k^2 + l_j^4 + 3l_j^2 l_k^2 - 2l_k^4}{12l_j^3 l_k^2} \underline{\varphi}_{\mathbf{n}_{T,e_j},1} + \frac{l_i^2 - l_j^2 + 3l_k^2}{40l_j l_k^2} \underline{\varphi}_{\mathbf{n}_{T,e_j},2} + \frac{1}{l_k} \underline{\varphi}_{\mathbf{n}_{T,e_k},0}.\end{aligned}$$

Then

$$\begin{aligned}\underline{W}_{T,e_j e_k}^{\mathbf{n}} &= \text{span}\{\underline{w}_{T,e_j}, \underline{w}_{T,e_j,e_k}, \underline{w}_{T,e_k,e_j}, \underline{w}_{T,e_k}\}, & \underline{W}_{T,e_k} &= \text{span}\{\underline{w}_{T,e_k}\}, \\ \text{and } \underline{W}_{T,e_j e_k} &= \text{span}\{\underline{w}_{T,e_j}, \underline{w}_{T,e_j,e_k}, \underline{w}_{T,e_k,e_j}, \underline{w}_{T,e_k}, \underline{w}_{T,a_i}\}.\end{aligned}$$

A.2. Divergence-free functions on sequentially connected cells. Let T_1 and T_2 be two adjacent cells such that $\overline{T_1} \cap \overline{T_2} = e_2$. Denote

$$\begin{aligned}\underline{V}_h(T_1 \cup T_2) &:= \{\underline{v}_h \in \underline{L}^2(T_1 \cup T_2) : \underline{v}_h|_{T_l} \in (P_2(T_l))^2, l = 1, 2, \\ &\quad \underline{v}_h \cdot \mathbf{n}_e \text{ and } \int_e \underline{v}_h \cdot \mathbf{t}_e ds \text{ are continuous across } e_2\},\end{aligned}$$

$$\underline{V}_{h0}(T_1 \cup T_2) := \{\underline{v}_h \in \underline{V}_h(T_1 \cup T_2) : \underline{v}_h \cdot \mathbf{n}_e \text{ and } \int_e \underline{v}_h \cdot \mathbf{t}_e \text{ vanish on } \partial(T_1 \cup T_2)\},$$

$$\underline{V}_{h,e_3}(T_1 \cup T_2) := \{\underline{v}_h \in \underline{V}_h(T_1 \cup T_2) : \underline{v}_h \cdot \mathbf{n}_e \text{ and } \int_e \underline{v}_h \cdot \mathbf{t}_e \text{ vanish on } \partial(T_1 \cup T_2) \setminus e_3\}.$$

Lemma A.2. *It holds that $\dim(\underline{V}_{h0}(T_1 \cup T_2)) = 0$ and $\dim(\underline{V}_{h,e_3}(T_1 \cup T_2)) = 2$.*



FIGURE 17. Two adjacent cells; Degrees of freedom vanish on dotted edges.

Proof. Given $\underline{\psi}_h \in \underline{V}_{h0}(T_1 \cup T_2)$, $\underline{\psi}_h|_{T_1} = \alpha \underline{w}_{T_1,e_2}$ and $\underline{\psi}_h|_{T_2} = \beta \underline{w}_{T_2,e_2}$. It is easy to verify that the weak continuity conditions imposed on e_2 makes $\alpha = \beta = 0$, namely $\underline{\psi}_h = \underline{0}$.

Similarly, we can prove $\dim(\underline{V}_{h,e_3}(T_1 \cup T_2)) = 2$. Specifically, two basis functions are

$$\underline{\psi}_h^1 \text{ such that } \underline{\psi}_h^1|_{T_1} = \underline{w}_{T_1,e_2} \text{ and } \underline{\psi}_h^1|_{T_2} = \underline{w}_{T_2,e_2} + \frac{S_1 + S_2}{d_2} \underline{w}_{T_2,e_3,e_2}$$

and

$$\underline{\psi}_h^2 \text{ such that } \underline{\psi}_h^2|_{T_1} = \underline{0} \text{ and } \underline{\psi}_h^2|_{T_2} = \underline{w}_{T_2,e_3}.$$

The proof is completed. \square

To admit a nontrivial basis function, at least four cells are needed.

Lemma A.3. *Let ω be a subdomain of three continuous cells, where the first and last cells are not connected; see Figure 18. If $\underline{v}_h \in \underline{V}_h(\omega)$, $\text{div}(\underline{v}_h) = 0$, and degrees of freedom of \underline{v}_h vanish on $\partial\omega$, then $\underline{v}_h = \underline{0}$.*

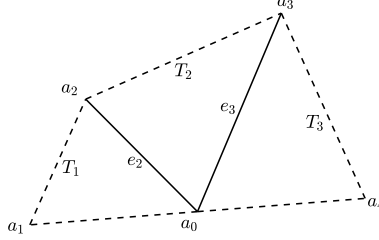


FIGURE 18. No trivial divergence-free function on three continuous cells.

Lemma A.4. *Let ω be a subdomain composed of four continuous cells, and its first and last cells are not connected; see Figure 19. A local space on ω is define as*

$$\underline{V}_{h0,\omega} := \left\{ \underline{v}_h \in \underline{L}^2(\omega) : \underline{v}_h|_T \in (P_2(T))^2, \forall T \in \omega, \underline{v}_h \cdot \mathbf{n}_e \text{ and } \int_e \underline{v}_h \cdot \mathbf{t}_e ds \text{ are continuous across interior edges and vanish on edges lying on } \partial\omega \right\},$$

then $\dim(\ker(\text{div}, \underline{V}_{h0,\omega})) = 1$.

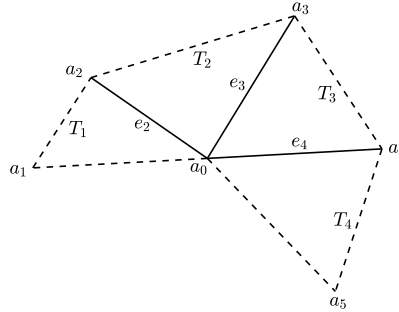


FIGURE 19. Patch ω composed of four continuous cells sharing an only vertex a_1 .

Proof. We will complete the proof in four steps.

Step 1. Consider T_1 and T_4 . We have

$$(A.4) \quad \underline{v}_h|_{T_1} = r \underline{w}_{T_1,e_2}, \quad \text{and} \quad \underline{v}_h|_{T_4} = s \underline{w}_{T_4,e_4}.$$

with constants r and s .

Step 2. Consider two adjacent cells $T_1 \cup T_2$. From Lemma A.2, it holds that

$$(A.5) \quad \underline{v}_h|_{T_2} = r \underline{w}_{T_2,e_2} + \left(\frac{S_1 + S_2}{d_2} r \right) \underline{w}_{T_2,e_3,e_2} + b_4 \underline{w}_{T_2,e_3}.$$

with b_4 to be determined.

Step 3. Consider two adjacent cells $T_3 \cup T_4$. Similar to Step 2, we have

$$(A.6) \quad \underline{v}_h|_{T_3} = c_1 \underline{w}_{T_3, e_3} - \left(\frac{S_4 + S_3}{d_4} s \right) \underline{w}_{T_3, e_3, e_4} + s \underline{w}_{T_3, e_4},$$

with c_1 to be determined.

Step 4. Consider two adjacent cells $T_2 \cup T_2$. Utilizing the continuity of $\underline{v}_h \cdot \mathbf{n}$ and $\int_{e_3} \underline{v}_h \cdot \mathbf{t}$ on e_3 , and the representation of \underline{v}_h in (A.4) – (A.6), we derive

$$(A.7) \quad b_4 = c_1 = 0, \quad s = -\frac{(S_1 + S_2)d_4}{(S_4 + S_3)d_2} r.$$

Therefore, \underline{v}_h is determined once the constant r is given and $\dim(\ker(\operatorname{div}, \underline{V}_{h0, \omega})) = 1$. \square

If we take $r = \frac{-d_2}{S_1 + S_2}$, then

$$(A.8) \quad \begin{aligned} \underline{v}_h|_{T_1} &= \frac{-d_2}{S_1 + S_2} \underline{w}_{T_1, e_2}, & \underline{v}_h|_{T_2} &= \frac{-d_2}{S_1 + S_2} \underline{w}_{T_2, e_2} - \underline{w}_{T_2, e_3, e_2}, \\ \underline{v}_h|_{T_3} &= -\underline{w}_{T_3, e_3, e_4} + \frac{d_4}{S_3 + S_4} \underline{w}_{T_3, e_4}, & \underline{v}_h|_{T_4} &= \frac{d_4}{S_3 + S_4} \underline{w}_{T_4, e_4}, \end{aligned}$$

Remark A.5. The pattern in Figure 18 can degenerate to a patch which admits only trivial function, i.e., zero vector function; see Figure 20.

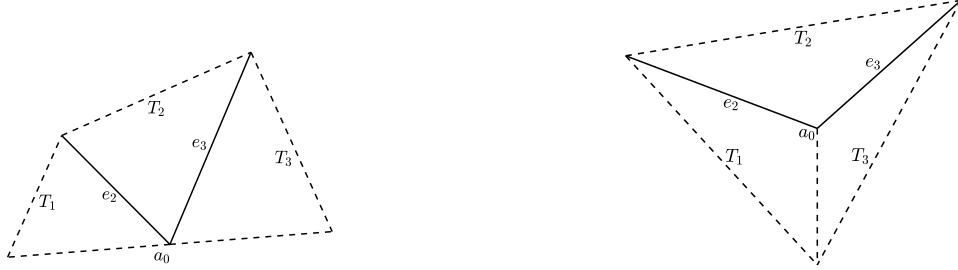


FIGURE 20. Degenerate case: three cells form a patch.

Remark A.6. Let T_1, T_2 and T_3 be three adjacent cells, such that $\bar{T}_1 \cap \bar{T}_2 = e_2$, $\bar{T}_2 \cap \bar{T}_3 = e_3$, and $\bar{T}_3 \cap \bar{T}_1 = e_1$. We may treat this triple of cells as a degenerate case of a four cell sequence $T_1 - T_2 - T_3 - T_1$, and the degenerate patch may inherit the divergence-free basis function on the patch $T_1 - T_2 - T_3 - T_1$.



FIGURE 21. The first and the last cells of the left pattern overlap to form the right pattern.

Take T_1 to be the overlapping cell. The function (corresponding to (A.8)), denoted by \underline{v}_1 , satisfies

$$(A.9) \quad \begin{aligned} \underline{v}_1|_{T_1} &= \frac{-d_2}{S_1 + S_2} \underline{w}_{T_1, e_2} + \frac{d_1}{S_3 + S_1} \underline{w}_{T_1, e_1} & \underline{v}_1|_{T_2} &= \frac{-d_2}{S_1 + S_2} \underline{w}_{T_2, e_2} - \underline{w}_{T_2, e_3, e_2}, \\ \underline{v}_1|_{T_3} &= -\underline{w}_{T_3, e_3, e_1} + \frac{d_1}{S_3 + S_1} \underline{w}_{T_3, e_1}. \end{aligned}$$

The key ingredient is that $\underline{v}_1|_{T_1}$ consists of \underline{w}_{T_1, e_2} and \underline{w}_{T_1, e_1} ; note that this is just the dominant ingredients of the function (corresponding to $T_1 - T_2 - T_3 - T_1$) on the two end cells.

A.3. Structure of the kernel space on an m -macroelement. Let $M = \cup_{s=1:m} T_s$ be an **m -macroelement**, and $\bar{T}_s \cap \bar{T}_{s+1} = e_{s+1}$. Particularly, $T_{m+1} = T_1$ and $e_{m+1} = e_1$. In the following context, the subscript s actually refers to $s - m$ if it is calculated to be great than m .

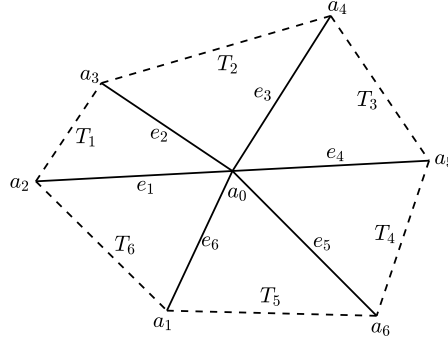


FIGURE 22. A macroelement composed of six cells with one interior vertex.

Definition A.7. Let a subdomain ω_l be composed of continuous cells $T_l \cup T_{l+1} \cup T_{l+2} \cup T_{l+3}$, and e_{l+1} , e_{l+2} , and e_{l+3} be its three interior edges. If

- (i) for $m \geq 4$, $\underline{v}_j|_{\omega_l} \in \ker(\operatorname{div}, \underline{V}_{h0, \omega_l})$ satisfies condition (A.8), and \underline{v}_j vanishes on $M \setminus \omega_l$,
- (ii) for $m = 3$, $\underline{v}_j|_{\omega_l} \in \ker(\operatorname{div}, \underline{V}_{h0, \omega_l})$ satisfies condition (A.9),

then \underline{v}_j is called an atom function on M .

Therefore, there exist m atom functions on an **m -macroelement**. Recall

$$(A.10) \quad \ker(\operatorname{div}, \underline{V}_{h0, M}) = \{ \underline{v}_h \in \underline{V}_{h0}(M) : \operatorname{div} \underline{v}_h = 0 \}$$

and denote

$$(A.11) \quad \underline{Z}_{h0}^n(M) := \{ \underline{v}_h \in \ker(\operatorname{div}, \underline{V}_{h0, M}) : \int_{e_i} \underline{v}_h \cdot \mathbf{n}_{e_i} = 0, 1 \leq i \leq m \}.$$

For an atom function \underline{v}_j on the **m -macroelement** M , $\operatorname{supp}(\underline{v}_j) := T_i \cup T_{i+1} \cup T_{i+2} \cup T_{i+3}$ ($m \geq 4$) or $\operatorname{supp}(\underline{v}_j) := T_i \cup T_{i+1} \cup T_{i+2}$ ($m = 3$). T_{i+s} is called the $(s + 1)$ -th cell of $\operatorname{supp}(\underline{v}_j)$.

Lemma A.8. *It holds that $\underline{Z}_{h0}^n(M) = \operatorname{span}\{\underline{v}_j\}_{1 \leq j \leq m}$.*

Proof. Here we adopt a sweeping procedure (c.f., Ref. [51]) to conduct the proof. Let T be an arbitrary cell in M , and $T_R \cup T \cup T_L$ be three cells in M arranged in a clockwise direction. Let $e_R := \bar{T}_R \cap \bar{T}$ and $e_L := \bar{T} \cap \bar{T}_L$. Use S_L and S_R to represent the areas of T_L and T_R , respectively. Let d_L and d_R represent the lengths of e_L and e_R .

Given $\underline{v}_h \in \underline{Z}_{h0}^n$, there exists $\alpha_i \in \mathbb{R}$, $1 \leq i \leq 4$, such that

$$\underline{v}_h|_T = \alpha_1 \underline{w}_{T,e_L} + \alpha_2 \underline{w}_{T,e_L,e_R} + \alpha_3 \underline{w}_{T,e_R,e_L} + \alpha_4 \underline{w}_{T,e_R}.$$

Let \underline{v}_{k_1} , \underline{v}_{k_2} , and \underline{v}_{k_3} be three atom functions satisfy that T is the first, second, and third cell of $\text{supp}(\underline{v}_{k_1})$, $\text{supp}(\underline{v}_{k_2})$, and $\text{supp}(\underline{v}_{k_3})$, respectively. Then

$$\begin{aligned} \underline{v}_{k_1}|_T &= \frac{-d_L}{S + S_L} \underline{w}_{T,e_L} \quad \text{or} \quad \underline{v}_{k_1}|_T = \frac{-d_L}{S + S_L} \underline{w}_{T,e_L} + \frac{d_R}{S + S_R} \underline{w}_{T,e_R} \quad \text{when } m = 3, \\ \underline{v}_{k_2}|_T &= \frac{-d_R}{S + S_R} \underline{w}_{T,e_R} - \underline{w}_{T,e_L,e_R}, \quad \underline{v}_{k_3}|_T = \frac{d_L}{S + S_L} \underline{w}_{T,e_L} - \underline{w}_{T,e_R,e_L}. \end{aligned}$$

Notice that $\underline{w}_{T,e_R}|_{e_L} = 0$ in the sense of DOF, i.e., the degrees of freedom associated with e_L of \underline{w}_{T,e_R} all vanish. Set

$$\underline{z}_0 = \left(-\alpha_1 \frac{S + S_L}{d_L} \underline{v}_{k_1} - \alpha_2 \underline{v}_{k_2} - \alpha_3 (\underline{v}_{k_1} + \underline{v}_{k_3}) \right) := r_1 \underline{v}_{k_1} + r_2 \underline{v}_{k_2} + r_3 \underline{v}_{k_3}.$$

then $(\underline{v}_h - \underline{z}_0)|_{e_L} = 0$ in the sense of DOF.

(i) If $m = 3$, it holds $\underline{v}_h - \underline{z}_0$ vanish on M by Remark A.5. Hence $\underline{v}_h = \sum_{l=1}^m r_l \underline{v}_{k_l}$.

(ii) If $m > 3$, consider the left cell T_L adjacent to T . There exists \underline{v}_{k_4} such that T_L is the first cell of $\text{supp}(\underline{v}_{k_4})$. Therefore, $(\underline{v}_h - \underline{z}_0)|_{T_L} \in \text{span}\{\underline{v}_{k_4}|_{T_L}\}$. Hence there exists a constant r_4 , such that $(\underline{v}_h - \underline{z}_0)|_{T_L} = r_4 \underline{v}_{k_4}$, and then $\underline{v}_h - \sum_{l=1}^4 r_l \underline{v}_{k_l}$ vanishes on T_L . Therefore, the number of supporting cells is reduced to $m - 1$. Conduct a similar analysis to the next left cell, and the number of supporting cells can also be reduced by one. Repeat this process until the number of supporting cells is smaller than three, and they form a pattern as shown in Figure 20 (left). Finally it can be derived that $\underline{v}_h = \sum_{l=1}^m r_l \underline{v}_{k_l}$. \square

Proof of Lemma 2.7. It suffices for us to show $\dim(\ker(\text{div}, \underline{V}_{h0,M})) \leq \dim(\underline{Z}_{h0}^n(M)) + 1$, and Lemma 2.7 follows by Lemma A.8.

Let \mathbf{n}_{e_l} be the unit normal vector on an interior edge e_l with $l = 1 : m$, whose direction is from a_0 to a_m . Given $\underline{\psi}_h \in \ker(\text{div}, \underline{V}_{h0,M})$, then the divergence theorem leads to $\int_{e_i} \underline{\psi}_h \cdot \mathbf{n}_{e_i} = \int_{e_j} \underline{\psi}_h \cdot \mathbf{n}_{e_j}$ with $1 \leq i, j \leq m$. Assume there exists a function $\underline{\psi}_h \in \ker(\text{div}, \underline{V}_{h0,M})$, such that $\int_{e_i} \underline{\psi}_h \cdot \mathbf{n}_{e_i} = 1$ with $i = 1 : m$. Then, $\underline{v}_h \in \ker(\text{div}, \underline{V}_{h0,M})$ can be uniquely decomposed into $\underline{v}_h = \alpha \underline{\psi}_h + \underline{v}_h^1$ with $\underline{v}_h^1 \in \underline{Z}_{h0}^n$, where α represents a constant. Namely, $\ker(\text{div}, \underline{V}_{h0,M}) = \underline{Z}_{h0}^n(M) + \text{span}\{\underline{\psi}_h\}$. If such a function $\underline{\psi}_h$ does not exist, then $\ker(\text{div}, \underline{V}_{h0,M}) = \underline{Z}_{h0}^n(M)$. In any event, $\dim(\ker(\text{div}, \underline{V}_{h0,M})) \leq \dim(\underline{Z}_{h0}^n(M)) + 1$. The proof is completed.

REFERENCES

- [1] D. N. Arnold and J. Qin. Quadratic velocity/linear pressure Stokes elements. In *Advances in Computer Methods for Partial Differential Equations VII*, pages 28–34. IMACS, 1992.
- [2] F. Auricchio, L. Beirão da Veiga, C. Lovadina, and A. Reali. The importance of the exact satisfaction of the incompressibility constraint in nonlinear elasticity: mixed FEMs versus NURBS-based approximations. *Computer Methods in Applied Mechanics and Engineering*, 199(5):314–323, 2010.
- [3] F. Auricchio, L. Beirão da Veiga, C. Lovadina, A. Reali, R. L. Taylor, and P. Wriggers. Approximation of incompressible large deformation elastic problems: some unresolved issues. *Computational Mechanics*, 52(5):1153–1167, 2013.
- [4] C. Bernardi and G. Raugel. Analysis of some finite elements for the Stokes problem. *Mathematics of Computation*, 44(169):71–79, 1985.

- [5] S. C. Brenner and L. R. Scott. *The mathematical theory of finite element methods*, volume 15 of *Texts in Applied Mathematics*. Springer-Verlag, New York, second edition, 2002.
- [6] F. Brezzi. On the existence, uniqueness and approximation of saddle-point problems arising from Lagrangian multipliers. *R.A.I.R.O. Analyse Numérique*, 8(R-2):129–151, 1974.
- [7] F. Brezzi, J. Douglas, Jr., and L. D. Marini. Recent results on mixed finite element methods for second order elliptic problems. In *Vistas in applied mathematics*, Transl. Ser. Math. Engrg., pages 25–43. Optimization Software, New York, 1986.
- [8] F. Brezzi and M. Fortin. *Mixed and Hybrid Finite Element Methods*, volume 15. Springer-Verlag, New York, 1991.
- [9] C.-H. Bruneau and M. Saad. The 2D lid-driven cavity problem revisited. *Computers & Fluids*, 35(3):326–348, 2006.
- [10] S. Chen, L. Dong, and Z. Qiao. Uniformly convergent $H(\text{div})$ -conforming rectangular elements for Darcy–Stokes problem. *Science China Mathematics*, 56(12):2723–2736, 2013.
- [11] P. G. Ciarlet. *The finite element method for elliptic problems*, volume 4. North-Holland Pub. Co, New York, Amsterdam, 1978.
- [12] M. Crouzeix and P.-A. Raviart. Conforming and nonconforming finite element methods for solving the stationary Stokes equations I. *R.A.I.R.O.*, 7(R3):33–75, 1973.
- [13] F. A. Dahlen. On the static deformation of an earth model with a fluid core. *Geophysical Journal of the Royal Astronomical Society*, 36(2):461–485, 1974.
- [14] B. A. D. Dios, F. Brezzi, L. D. Marini, J. Xu, and L. Zikatanov. A simple preconditioner for a discontinuous Galerkin method for the Stokes problem. *Journal of Scientific Computing*, 58(3):517–547, 2014.
- [15] R. S. Falk and E. Morley. Equivalence of finite element methods for problems in elasticity. *SIAM Journal on Numerical Analysis*, 27:1486–1505, 1990.
- [16] R. S. Falk and M. Neilan. Stokes complexes and the construction of stable finite elements with pointwise mass conservation. *SIAM Journal on Numerical Analysis*, 51(2):1308–1326, 2013.
- [17] M. Fortin. An analysis of the convergence of mixed finite element methods. *RAIRO Analyse Numérique*, 11(4):341–354, 1977.
- [18] N. R. Gauger, A. Linke, and P. W. Schroeder. On high-order pressure-robust space discretisations, their advantages for incompressible high Reynolds number generalised Beltrami flows and beyond. *The SMAI Journal of Computational Mathematics*, 5:89–129, 2019.
- [19] V. Girault and P.-A. Raviart. *Finite element methods for Navier–Stokes equations*, volume 5 of *Springer Series in Computational Mathematics*. Springer-Verlag, Berlin, 1986.
- [20] J. Guzmán and M. Neilan. A family of nonconforming elements for the Brinkman problem. *IMA Journal of Numerical Analysis*, 32(4):1484–1508, 2012.
- [21] J. Guzmán and M. Neilan. Conforming and divergence-free Stokes elements in three dimensions. *IMA Journal of Numerical Analysis*, 34:1489–1508, 10 2013.
- [22] J. Guzmán and M. Neilan. Conforming and divergence-free Stokes elements on general triangular meshes. *Mathematics of Computation*, 83(285):15–36, 2014.
- [23] J. Guzmán and M. Neilan. Inf-sup stable finite elements on barycentric refinements producing divergence-free approximations in arbitrary dimensions. *SIAM Journal on Numerical Analysis*, 56(5):2826–2844, 2018.
- [24] R. Hiptmair, L. Li, S. Mao, and W. Zheng. A fully divergence-free finite element method for magnetohydrodynamic equations. *Mathematical Models and Methods in Applied Sciences*, 28:1–37, 2018.
- [25] Q. Hong, F. Wang, S. Wu, and J. Xu. A unified study of continuous and discontinuous Galerkin methods. *Science China. Mathematics*, 62(1):1–32, 2019.
- [26] K. Hu, Y. Ma, and J. Xu. Stable finite element methods preserving $\nabla \cdot \mathbf{B} = 0$ exactly for MHD models. *Numerische Mathematik*, 135(2):371–396, 2017.
- [27] K. Hu and J. Xu. Structure-preserving finite element methods for stationary MHD models. *Mathematics of Computation*, 88(316):553–581, 03 2019.
- [28] Y. Huang and S. Zhang. A lowest order divergence-free finite element on rectangular grids. *Frontiers of Mathematics in China*, 6(002):253–270, 2011.
- [29] V. John, A. Linke, C. Merdon, M. Neilan, and L. G. Rebholz. On the divergence constraint in mixed finite element methods for incompressible flows. *SIAM Review*, 59(3):492–544, 2017.

- [30] R. Kouhia and R. Stenberg. A linear nonconforming finite element method for nearly incompressible elasticity and Stokes flow. *Computer Methods in Applied Mechanics & Engineering*, 124(3):195–212, 1995.
- [31] A. Linke and C. Merdon. Well-balanced discretisation for the compressible Stokes problem by gradient-robustness. In R. Klöforn, E. Keilegavlen, F. A. Radu, and J. Fuhrmann, editors, *Finite Volumes for Complex Applications IX - Methods, Theoretical Aspects, Examples*, pages 113–121, Cham, 2020. Springer International Publishing.
- [32] A. Linke and L. G. Rebholz. Pressure-induced locking in mixed methods for time-dependent (Navier–)Stokes equations. *Journal of Computational Physics*, 388:350 – 356, 2019.
- [33] K. A. Mardal, X.-C. Tai, and R. Winther. A robust finite element method for Darcy–Stokes flow. *SIAM Journal on Numerical Analysis*, 40(5):1605–1631, 2002.
- [34] M. Neilan and D. Sap. Stokes elements on cubic meshes yielding divergence-free approximations. *Calcolo*, 53(3):263–283, 2016.
- [35] J. Qin and S. Zhang. Stability and approximability of the $P_1 - P_0$ element for Stokes equations. *International Journal for Numerical Methods in Fluids*, 54(5):497–515, 2007.
- [36] P. W. Schroeder and G. Lube. Divergence-free H(div)-FEM for time-dependent incompressible flows with applications to high Reynolds number vortex dynamics. *Journal of Scientific Computing*, 75:830–858, 05 2018.
- [37] L. R. Scott and M. Vogelius. Norm estimates for a maximal right inverse of the divergence operator in spaces of piecewise polynomials. *RAIRO Modélisation Mathématique et Analyse Numérique*, 19(1):111–143, 2009.
- [38] R. Stenberg. A technique for analysing finite element methods for viscous incompressible flow. *International Journal for Numerical Methods in Fluids*, 11(6):935–948, 1990.
- [39] X.-C. Tai and R. Winther. A discrete de Rham complex with enhanced smoothness. *Calcolo*, 43(4):287–306, 2006.
- [40] S. Uchiumi. A viscosity-independent error estimate of a pressure-stabilized Lagrange-Galerkin scheme for the Oseen problem. *Journal of Scientific Computing*, 80(2):834–858, 2019.
- [41] X. Xie, J. Xu, and G. Xue. Uniformly stable finite element methods for Darcy–Stokes–Brinkman models. *Journal of Computational Mathematics*, 26(3):437–455, 05 2008.
- [42] J. Xu. Iterative methods by space decomposition and subspace correction. *SIAM Review*, 34(4):581–613, 1992.
- [43] X. Xu and S. Zhang. A new divergence-free interpolation operator with applications to the Darcy–Stokes–Brinkman equations. *SIAM Journal on Scientific Computing*, 32(2):855–874, 2010.
- [44] H. Zeng, C.-S. Zhang, and S. Zhang. Optimal quadratic element on rectangular grids for H^1 problems. *BIT Numerical Mathematics*, published online, 2020.
- [45] S. Zhang. A new family of stable mixed finite elements for the 3D Stokes equations. *Mathematics of Computation*, 74(250):543–554, 2005.
- [46] S. Zhang. On the P_1 Powell-Sabin divergence-free finite element for the Stokes equations. *Journal of Computational Mathematics*, 26(003):456–470, 2008.
- [47] S. Zhang. A family of $Q_{k+1,k} \times Q_{k,k+1}$ divergence-free finite elements on rectangular grids. *SIAM Journal on Numerical Analysis*, 47(3):2090–2107, 01 2009.
- [48] S. Zhang. Divergence-free finite elements on tetrahedral grids for $k \geq 6$. *Mathematics of Computation*, 80(274):669–695, 2011.
- [49] S. Zhang. Quadratic divergence-free finite elements on Powell–Sabin tetrahedral grids. *Calcolo*, 48(3):211–244, Sept. 2011.
- [50] S. Zhang. Stable finite element pair for stokes problem and discrete stokes complex on quadrilateral grids. *Numerische Mathematik*, 133:371–408, 2016.
- [51] S. Zhang. Minimal consistent finite element space for the biharmonic equation on quadrilateral grids. *IMA Journal of Numerical Analysis*, 40(2):1390–1406, 2020.

LSEC, INSTITUTE OF COMPUTATIONAL MATHEMATICS AND SCIENTIFIC/ENGINEERING COMPUTATION, ACADEMY OF MATHEMATICS AND SYSTEM SCIENCES, CHINESE ACADEMY OF SCIENCES, BEIJING 100190, CHINA; UNIVERSITY OF CHINESE ACADEMY OF SCIENCES, BEIJING 100049, CHINA

Email address: {zh1, zhangcs, szhang}@lsec.cc.ac.cn